SKB

TECHNICAL REPORT

92-11

Numerical groundwater flow calculations at the Finnsjön study site – the influence of the regional gradient

Björn Lindbom
Anders Boghammar

Kemakta Consultants Co., Stockholm Sweden

April 1992

NUMERICAL GROUNDWATER FLOW CALCULATIONS AT THE
FINNSJÖN STUDY SITE -
THE INFLUENCE OF THE REGIONAL GRADIENT

Björn Lindbom, Anders Boghammar

Kemakta Consultants Co., Stockholm, Sweden

April 1992

Numerical groundwater flow calculations at the Finnsjön study site – the influence of the regional gradient

by

Björn Lindbom
Anders Boghammar

Kemakta Consultants Co.
Pipersgatan 27
112 28 Stockholm, Sweden

Abstract

The present report describes the modelling efforts of the groundwater flow situation at the Finnsjön site in northern Uppland, approximately 140 km north of Stockholm. The study forms part of the SKB 91 performance assessment project, and aims at describing the model sensitivity to changes in the prevailing regional gradient, as well as the local, with regard to both direction and magnitude. Particular emphasis has been put into the evaluation of travel times and travel paths from a potential repository, and also on flux values at repository level. The analyses were based on the finite element technique and made use of the NAMMU-code for stationary calculations in three dimensions.

The fracture zones within the modelled area were modelled implicitly with an averaging technique.

Stockholm, April, 1992.

Summary

The present study forms part of the SKB 91 performance assessment project. It is devoted to numerical groundwater flow calculations at the Finnsjön study site and forms part of a series of studies aiming at the description of the groundwater flow situation at the site.

The present study aims at identifying the influence of the regional gradient (on a 10 km-scale) from two angles; partly in order to see at what magnitude the regional gradient eliminates the natural discharge areas by over-riding the natural groundwater topography, and partly in order to disturb the natural recharge conditions over the major sub-horizontal zone 2 by changing the natural local gradient (on a 1 km-scale) particularly in the area where the impact from zone 2 is strongest. The latter is of interest since the repository is located below zone 2, and the former since it includes a study of the discharge area, i.e where biological life is assumed to be exposed to a potential radioactive dose.

Thus, two different model set-ups were analysed, one with a W-E oriented regional gradient, and one with a SW-NE oriented regional gradient added to the natural groundwater table.

By varying the additional W-E gradient, it could be seen that the discharge took place at about the same position as under natural conditions, provided that the imposed gradient was not too large. Despite that the imposed gradient when directed W-E, to some extent counteracted the one over the discharge area, the model turned out to be fairly insensitive to the disturbed conditions. A span between roughly twice and half the natural gradient appeared to imply that the discharge took place at roughly the same positions as under natural conditions. However, an imposed gradient being roughly four times as high as the natural one made the particles be discharged at another location, a process which was also reinforced by the gradient acting over the repository area. The conclusion to be drawn is that the magnitude of the imposed gradient probably sets some kind of a limit to when the Imundbo zone can be regarded as the discharge area. The uncertainty span corresponds to a change in surficial altitude of the groundwater table of about 8 m in the area around the Imundbo zone and roughly 12 m at the west-most model boundary. These deviations could be caused by malfunctions of field equipment, seasonal variations, or any disturbance introduced by man.

Three calculation cases were analysed with varying degree of disturbance of a topography plane that was fixed along a line parallel to the southern part of the Imundbo zone. One case with an applied regional gradient so that the resulting SW-NE directed local scale gradient was doubled compared to the natural one, indicated that all the particles were discharged in the upper NE corner of the modelled domain. A second case with a resulting local gradient largely reduced showed a wide spread in discharge locations for the particles. Some of the released particles turned southward directly after them being released. The third case, with an imposed gradient so that the resulting local gradient was about 75% of the natural one, indicated that the particles now approached their natural discharge area, the Imundbo zone. This leads to the conclusion that an applied regional gradient in the order of about 75-100% of the natural one, yields in a discharge at locations that can be regarded as the natural ones. The low end of the span implied that the groundwater table was lowered with about 8-10 m over the potential repository area, with in principle a maintained discharge area. The distribution of pathlines for this set of cases indicated that the imposed gradient to a larger extent coincided with the natural one than was the situation for the cases mentioned above.

Conclusively, one could state that the flow in the repository area is governed by both the local and regional gradient, to a larger extent than the neighbourhood of the discharge area. This depended mainly on that the imposed gradients counteracted the discharge area gradient more than the gradient over the repository area. The gradient in the latter area sometimes interacted with the imposed gradient.

Table of Contents

1. Introduction

1.1 Purpose and Scope of the Project

The present project forms part of the SKB 91 performance assessment project. It is devoted to numerical groundwater flow calculations at the Finnsjön study site and forms part of a series of studies aiming at the description of the groundwater flow situation at the site.

Parallel and previous studies (KEM1, 1992 and KEM2, 1991) have indicated that a) the major discharge takes place in the vicinity (and in) the regional lineament Imundbo, and b) the recharge of interest in this context takes place over zone 2, and by this over the repository. The present study therefore aims at identifying the importance of the regional gradient relative to the importance of the gradient over the Imundbo zone and over the repository area. The means are to impose a regional gradient, and to analyse at what magnitude and direction the flow conditions are substantially changed.

The origin of the background data is (SGAB1, 1991), while the data as interpreted for modelling purposes can be found in (KEM2, 1991). The extension of the regional scale model in the KEM2-study was smaller than that considered in the present project. The extended area incorporated the modelling of three more zones, that were located outside the previously modelled area, see Figure 1.1. The fracture zones were modelled implicitly with an averaging technique developed by Kemakta in the IFZ-code (KEM2, 1991).

In order to facilitate comparisons with the results from the main study (KEM1, 1992), the major results and conclusions are more or less copied and included in the present report.

The calculations have been performed in three dimensions and made use of the NAMMU-package (HARW1, 1979 and HARW2, 1985) for solving the equation system (finite element technique), while the HYPAC-package (KEM3, 1989) was used for pre- and postprocessing purposes.

NAMMU is implemented on a Convex, model C-220. The calculations performed within this project were carried out in three dimensions with 8-noded brick elements, which means that the interpolation between element corners is linear. NAMMU version 4S has been used within the present project.

The particle tracking as presented in the report is based on a Euler technique, i.e. with a simple forward stepping. The step-length is specified by the user; the tracking routine forms part of the HYPAC program package, (KEM2, 1989).

The entity "flux" ($\bar{q}$) as reported in the study, equal to the "Darcy velocity" or the "volumetric flux", is expressed in $m^3/m^2/year$, and is calculated according to the formula:

$$|\bar{q}| = \sqrt{q_x^2 + q_y^2 + q_z^2},$$

where x, y, and z denotes the directions of the cartesian coordinates in meters.

The coordinate system used is the RAK-system with an offset in y=1600000 m and x=660000 m, the same offset as used in (SGAB1, 1991).

2. Hydraulic Properties – Boundary Conditions – Case Descriptions

The increased areal extension of the model has incorporated a few fracture zones that were not included in the KEM2-study. These fracture zones are from now on referred to as zones Giboda S, NS1 and NS2, see Figure 1.1 for their locations. Their hydraulic properties were judged according to their nearness to the Giboda zone and zone 4 for zone Giboda S, and the similarity between zone 12 and zones NS1 and NS2 (SGAB2, 1991).

The geometries and properties of the fracture zones were kept constant throughout the study, and are shown in Table 2.1. The conductivities for both the rock mass and the fracture zones were assumed to obey the formula $K=a \cdot z^{-b}$, where K denotes the hydraulic conductivity (m/s). The value of the factor "a" is given for each fracture zone in Table 2.1. All fracture zones and the rock mass are assumed to have the same depth dependence with the exponent "b" equal to 2.23. The value of the factor "a" is equal to 0.0121 for the rock mass.

Table 2.1   *Fracture zones in the Finnsjön area as modelled within the present project. For further information with regard to background values, see (SGAB1, 1991). The abbreviations for the regional lineaments in the table refer to their notations in Figure 2.2.*

Zone	Width (m)	Inclination (degrees)	Factor "a"
1	20	75 SE	0.187
2	100	16 SW	0.427
3	50	80 SW	0.140
4	10	60 SW	0.118
12[1]	50	90	0.118
13[2]	50	90	0.187
14[1]	50	90	0.118
Skogsbo (Sk)[3]	100	90	0.270
Giboda (Gi)[3]	100	90	0.270
Imundbo (Im)[3]	100	90	0.270
Gräsbo (Gr)[1]	100	90	0.118
Dannemora (Da)[1]	100	90	0.118
Källviken (Kä)[2]	100	90	0.187
Giboda S (GiS)[4]	50	90	0.270
NS1 (NS1)[5]	50	90	0.118
NS2[2] (NS2)[6]	25	90	0.118

[1]   *Hydraulic properties assumed to be similar to those of the Singö-fault, see (SGAB1, 1991).*
[2]   *Hydraulic properties assumed to be similar to those of zone 1.*
[3]   *Hydraulic properties assumed to be similar to those of local fracture zone 5, see (SGAB1, 1991).*
[4]   *The zone is assumed to have the same hydraulic properties as the Giboda zone, but with an intermediate width between zone 4 and the Giboda zone.*
[5]   *The zone is assumed to have the same hydraulic properties as zone 12.*
[6]   *The zone is assumed to have the same hydraulic properties as zone 12, but with a different width.*

The lateral and bottom boundaries were of no-flow type, whereas the upper boundary condition (i.e. the position of the groundwater table) was of a prescribed "zero-pressure" type. The natural groundwater table is shown in Figure 2.1.

The depth dependence of the rock mass conductivity and the fracture zone conductivities are shown in Figure 2.2. A top view of the finite element mesh that was generated is shown in Figure 2.4. The mesh contains about 18400 eight-noded brick elements, with a total of about 20700 nodes.

Of utmost interest in the context of disposal of radioactive waste are the conditions in the discharge area, and the transport times from the repository to the discharge area. A prerequisite for discharge to take place, is that recharge occurs elsewhere in the domain, thus supplying a driving force. Therefore, it is essential to investigate the flow conditions in both recharge and discharge areas. To this end, two series of calculations were set up within the present study. These aimed at identifying the sensitivity of the model results to flow directions and transport times to the discharge areas with respect to the changes in the local gradient over the repository area, and to the changes in the gradient over the discharge area caused by a change in the prevailing regional gradient. Both series included a manipulation of the natural groundwater topography by imposing a linearly increasing or decreasing topography added to the natural one. This procedure implies that local fluctuations in the natural groundwater table are diminished by increasing deviation from the natural groundwater topography.

Two calculation series were formulated so that either the regional gradient in the W–E-direction was changed (measured from point A to C in Figure 2.1), or so that the SW–NE-directed regional gradient was changed (measured from point A to D in Figure 2.1). Of interest was to analyse the changes of the local gradient over the repository area and the changes of the regional gradient over the discharge area that was caused by the imposed gradients as described above.

Sensitivity to W-E regional gradient

The "topography plane" that is added to the natural one is fixed along the Dannemora zone (points A-B), a hinge where the plane is allowed to rotate. The intention was to study the persistence of the discharge area around the Imundbo zone when a regional gradient other than the natural one is prevailing. The natural regional gradient measured from point A to C in Figure 2.1 is roughly 0.17%. Three variations were considered by adding a "topography plane" so that the regional gradient between these points was gradually increased. These cases were denoted X36GRV1, X36GRV2, and X36GRV3, respectively. The resulting local gradient over the northern local scale block (i.e. roughly corresponding to the repository area), and the resulting regional gradient over the discharge area was estimated for the different cases. The local repository-area gradient was measured between points D and E, while the gradient over the discharge area was measured between points E and F. See Table 2.2 for a collection of the imposed gradients for the different set-ups.

Table 2.2 also contains a calculation of the ratio of the gradient over the distances in question, for the different cases. This value gives an idea on how large the deviation is from the natural flow conditions.

Sensitivity to SW-NE regional gradient

The "topography plane" that is added to the natural one is fixed in point A along a line being parallel to the southern part of the Imundbo zone, see Figure 2.1. The intention with this analysis was to study the impact on the discharge as a result of a disturbance over the recharge area with a regional gradient other than the natural one prevailing. The regional gradient was measured from point A to point D, while the local repository-area gradient was measured between points D-E. The gradient over the discharge area was measured between points E-F. The natural regional gradient over the distance according to above was about 0.20%. Three variations were considered also here, denoted X36GRV4, X36GRV5 and X36GRV6, respectively. Table 2.3 contains the added and resulting gradients, as well as the ratios of the gradients over the distances in question, for the different cases.

Table 2.2   *Regional and local gradients (in %) for Cases X36GRV1, X36GRV2 and X36GRV3 as a result of an imposed gradient along a plane fixed in a line between points A and B, see Figure 2.1.*

Case		Gradient over distance				Ratio DE/EF	Ratio AC/EF	Ratio AC/DE
		A-C	A-D	D-E	E-F			
Natural		0.17	0.20	0.57	0.16	3.6	1.0	0.3
X36GRV1	added	0.25	0.20	0.32	-0.14			
	resulting	0.42	0.40	0.89	0.02	44.5	20.5	0.5
X36GRV2	added	0.48	0.40	0.57	-0.07			
	resulting	0.65	0.60	1.14	0.09	12.6	7.1	0.6
X36GRV3	added	0.13	0.10	0.13	-0.07			
	resulting	0.30	0.30	0.70	0.09	7.8	3.2	0.4

Table 2.3   *Regional and local gradients (in %) for Cases X36GRV4, X36GRV5 and X36GRV6 as a result of an imposed gradient along a plane through point A and fixed in a line parallel to the southern part of the Imundbo zone, see Figure 2.1.*

Case		Gradient over distance				Ratio DE/EF	Ratio AD/EF	Ratio AD/DE
		A-C	A-D	D-E	E-F			
Natural		0.17	0.20	0.57	0.16	3.6	1.3	0.4
X36GRV4	added	0.42	0.62	0.96	0.48			
	resulting	0.59	0.82	1.53	0.64	2.4	1.3	0.5
X36GRV5	added	-0.27	-0.30	-0.73	-0.10			
	resulting	-0.10	-0.10	-0.16	-0.06	2.7	1.7	0.6
X36GRV6	added	-0.15	-0.16	-0.22	-0.02			
	resulting	0.02	0.04	0.35	0.14	2.5	0.3	0.1

3. Modelling Results

The evaluation in a general sense is somewhat more extensive in the KEM1-study than that reported in the present report. The present study is focussed on the evaluation of particle tracking and the distribution of fluxes at repository level. For comparison with the main case, Case X36 in the KEM1-study, some selected results from that report is included (without comments) in this report.

The evaluation comprises particle tracking (including visual presentation of the particle tracks and table-wise collections of travel times and travel lengths) and flux distribution at repository level (presented as a cumulative diagram). Repository level is assumed to be at z=-600 m, a level where the particles are released.

Since the study involves the assignment of a groundwater topography different from the natural one, the presentation also includes a top view of the distribution of the hydraulic head at the top surface for each of the cases studied below.

In order to reduce the volume of the main report, some of the evaluation figures have been moved to Appendix B.

For comparison, the results for the Base Case (Case X36) from (KEM1, 1992) are included below. These are shown in Section 3.1, while the influence from a WE-directed fictive regional gradient is discussed in Section 3.2.1 and the influence from a SW–NE-directed gradient is discussed in Section 3.2.2.

3.1 Case X36 – the Base Case

Distribution of hydraulic head at the level z=0 m is shown in Figure 3.1.

Flux distribution in a cumulative diagram is shown in Figure 3.2.

Particle Tracking (horizontal projection) is shown in Figure 3.3. Vertical projections of pathlines are shown in Appendix B. Accumulated travel times and travel lengths are collected in Table 3.1.

Table 3.1 Accumulated travel times (ACT) in years, and accumulated travel lengths (ACL) in metres for Case X36. The particles were released at 600 m depth. A porosity of 0.0001 has been assumed when travel times were calculated.

Path no	ACT	ACL
1	485	5600
2	250	5580
3	170	5880
4	265	5780
5	350	5890
6	540	6050
7	550	6140
8	1000	6460

3.2   Influence from the Regional Gradient

3.2.1   Regional Gradient in W–E-direction

Imposed gradient at top surface

Three situations were studied with different magnitude of the imposed regional gradient. Figures 3.4, 3.5 and 3.6 show the hydraulic head distributions at z=0 m for Cases X36GRV1, X36GRV2 and X36GRV3, respectively. The natural regional gradient is roughly 0.23% measured from the Dannemora zone to the lower left hand corner of the area indicated in Figure 2.1 between points A and C.

Particle Tracking

The vertical projections of the resulting flow paths for the eight particles that were released from the potential repository are shown in Appendix B. Figures 3.7, 3.8, and 3.9 show the horizontal projection of the pathlines for Cases X36GRV1, X36GRV2 and X36GRV3, respectively. This series of figures shows that the discharge takes place in the Dannemora zone. The more certainty can obviously be put into this statement with increasing magnitude of the imposed regional gradient.

Figure 3.10 shows the horizontal projection for one representative particle path (number 7) for all the three different situations described above; for comparison the resulting path way for Case X36 is included. Evidently, the particles tend to go to the Dannemora zone with increasing emphasis with increasing magnitude of the imposed gradient. Under natural conditions, like in Case X36, the flow is governed by a regional SW-NE-directed gradient, to be replaced by a local SE–NW-directed one in the vicinity of the Imundbo zone. The imposed gradient (measured from A to C in Figure 2.1) for Cases X36GRV1 and X36GRV2 is apparently high enough to over-ride the natural flow field, whereas Case X36GRV3 reflects an intermediate situation, where the natural SW-NE-oriented gradient forces the particles to the Imundbo zone. Once they enter their natural discharge area here, they are simultaneously subjected to the natural local SE-NW-directed gradient and the imposed artificial gradient in the W–E-direction. These two directions counteract with a resulting discharge in the area where the particles normally enter the Imundbo zone. This is further illustrated in Figure 3.11, showing one of the vertical projections (the yz-plane) of pathline 7.

The travel times and travel lengths for all particles for the three situations are collected in Table 3.2 below (for comparison with Case X36, see Table 3.1). The travel times for Case X36GRV3 are slightly shorter than for Case X36, whereas the travel times are significantly shorter. This depends on the earlier discharge for this case than for Case X36. The two remaining cases with a gradient higher (over the A-C distance) than the natural one show travel times that are roughly 40% faster for Case X36GRV1 and roughly the same for Case X36GRV3, compared to Case X36. The latter may seem a bit surprising, but can be explained by the deeper flow paths for this case, which in turn is caused by the higher gradient imposed. This is also confirmed by the longer travel lengths for this case compared to Case X36GRV1.

Conclusively, the imposed gradient along line A-C has affected (and counteracted) the gradient over the discharge area more than it did the gradient over the repository area. The natural gradient over the repository area is closer to coincide with the imposed one than the natural gradient over the discharge area. This is also confirmed by the ratio-values given in Table 3.2, where the imposed gradient along line A-C implied a lowering of the gradient over the discharge area, as opposed to the situation over the repository area. The relationship between the imposed gradient and the one over the repository area is also visible as small deviations in the "ratio-column" in Table 3.2 for these two lines; when the ratio is lower than 0.4, the flow is discharged roughly at the same locations as for the Base Case (Case X36), whereas ratio-values larger than 0.4 implies that the interacting imposed and repository-area gradient have a stronger influence on the discharge system than the prevailing gradient over the discharge area itself (the gradient over the discharge area is the same for Case X36GRV2 as for Case X36GRV3).

Table 3.2   *Accumulated travel times (ACT) in years and travel lengths (ACL) in meters for the three cases considered. Porosity assumed to be 0.0001.*

Case:	X36GRV1		X36GRV2		X36GRV3	
Path no	ACT	ACL	ACT	ACL	ACT	ACL
1	179	3710	276	8240	332	4050
2	158	3470	265	7920	179	3310
3	147	3110	371	7880	157	2500
4	196	3490	469	8210	258	3010
5	453	8260	771	8370	293	2990
6	252	3830	469	8550	349	3800
7	463	8680	742	8550	390	3220
8	1243	8440	1443	5620	707	5220

Flux distribution

Figure 3.12 shows the cumulative flux distribution over the potential repository area as calculated for the three cases (for comparison, the results for Case X36 are included in the same plot). The figure shows that the fluxes at repository level increase approximately linearly with increasing gradient, which only confirms the use of the Darcy law. The highest median value of about 0.002 m^3/m^2/year is seen for Case X36GRV2, while the lowest median value is obtained for Case X36, roughly 0.001 m^3/m^2/year. The two remaining cases have values between these two.

3.2.2 Regional Gradient in SW–NE-direction

Imposed gradient at top surface

Three situations were studied also here with different magnitude of the imposed regional gradient. Figures 3.13, 3.14 and 3.15 show the hydraulic head distributions at z=0 m for Cases X36GRV4, X36GRV5 and X36GRV6. The natural gradient is about 0.20%, and is measured over the area between the Imundbo zone and a point in the middle of the repository area (points D-E in Figure 2.1).

Particle Tracking

The vertical projections of the resulting flow paths for the eight particles that were released from the potential repository are shown in Appendix B. Figures 3.16, 3.17, and 3.18 show the horizontal projection of the pathlines for Cases X36GRV4, X36GRV5 and X36GRV6, respectively. This series shows somewhat more disparate pathlines than was the situation with a W-E-directed regional gradient as described in the previous Section. The pathlines for Case X36GRV4 (with an imposed regional gradient roughly three times the natural one) illustrates clearly that the imposed gradient over-rides the natural one (measured over the distance A-D) in that the pathlines are discharged at the model boundary in the NE corner; seemingly unaffected by the presence of the Imundbo zone. On the other hand, the pathlines appear to be affected by the Giboda zone, which can be seen as a narrow band where the particles travel in a W–E-direction prior to them being discharged. The particles for Case X36GRV5 show a completely different pattern, which depends on that the additional topography plane has implied a reduction of the regional gradient so that the prevailing gradient has been lowered enough to make the flow pattern change direction as seen from the repository area. From Figure 3.17 (compare also with Figure 3.14) it is evident that the particles

within the potential repository area are released in the vicinity of a water divide which in a sense reflects that the prevailing local gradient in the repository area has a stronger impact than the regional gradient. A majority of the pathlines turn in a SW direction instead of the natural NE direction. As can be seen in Appendix B in the Figures showing the vertical projections of the pathlines, only a couple of them reached the ground surface, the remaining ones were aborted prior to their discharge. The reason for this could be too low a gradient to create a driving force for the flow. The particles for Case X36GRV6 show an intermediate reaction to the imposed gradient. The reason is two-fold; the imposed regional gradient has resulted in a reduction of the natural one, which implies that the discharge area has been moved westward (the area west of the Imundbo zone is located lower than in Case X36). The second reason is that the flow from the peak in the angle between the Dannemora zone and the Imundbo zone (Gullbacken) is affected less (in relative terms) by the reduction of the natural regional gradient, since the peak is located closer to the "hinge" than the discharge area. The majority of the particles appear to approach what can be called the natural discharge area, although the resulting pathlines do not coincide perfectly with the ones for Case X36. One of the particles (number 8) is still being discharged in a SW direction, which depends on that it is being released on the south side of the water divide within the repository area.

Figure 3.19 shows the horizontal projection for one representative particle path (number 7) for all the three different situations described above, while Figure 3.20 shows the vertical projection (yz-plane) of the same particle for al three cases. For comparison the resulting path way for Case X36 is included. Both these figures reflect the situation as described above in an illustrative manner.

The travel times and travel lengths for all particles for the three situations are collected in Table 3.3 below (for comparison with Case X36, see Table 3.1). The high gradient case (Case X36GRV4) clearly reflect the situation; by far the longest travel lengths and shortest travel times; all particles are discharged at about the same location with average travel lengths of roughly 8700 m and average travel times of about 240 years. The indifferent low-gradient situation is seen for Case X36GRV5, with short travel lengths (average of about 2300 m) and a wide spread in travel times ranging from 200 years to 2500 years, in average roughly 950 years. Finally, Case X36GRV6 reflects an intermediate situation with average travel times of about 880 years and travel lengths of roughly 4100 m. This case also proved to have a wide spread in travel times, reflecting the somewhat "unstable" situation if compared to Case X36GRV4.

The imposed gradient for these cases is coinciding with the natural regional prevailing gradient more than was the situation as described in Section 3.2.1. This conclusion can be drawn by studying the ratio-values given in Table 3.3, where it turns out that all these values are affected to a much lesser extent than previously discussed. However, the discharge under natural conditions is governed by a local SE-NW-directed gradient over the Imundbo zone, which is strongly affected by the imposed gradient; almost a perfect counteraction between these two directions is found. However, even at small gradients over the repository area, the water particles are discharged in the vicinity of the natural discharge location. This depends on that the influence from the Gullbacken peak is stronger in relative terms spoken, than the situation when large gradients are imposed over the area. This is seen as a re-establishment of the natural pressure distribution in some sense which puts the discharge area around the Imundbo zone back in position as the major discharge area (Case X36GRV6).

Table 3.3   Accumulated travel times (ACT) in years and travel lengths (ACL) in meters for the three cases considered. Porosity assumed to be 0.0001.

Case:	X36GRV4		X36GRV5		X36GRV6	
Path no	ACT	ACL	ACT	ACL	ACT	ACL
1	333	8460	2527	1190	774	4100
2	260	8530	1655	3870	587	4340
3	139	8410	929	4010	284	2790
4	179	8660	1240	2570	894	4640
5	193	8770	967	2160	834	4010
6	293	8960	485	2020	1658	4840
7	174	8870	396	1620	2914	5980
8	387	9200	200	1600	558	1930

Flux distribution

The flux distribution over the repository area is shown in Figure 3.21 for the three cases. For comparison, the results for Case X36 are also included. The median value for Case X36GRV4 is roughly 0.002 m^3/m2/year, i.e. an increase of a factor 2 compared to Case X36. The two remaining cases show flux values that are lower than those for Case X36, since the imposed regional gradient is lower than the natural one for these two cases; the median values for the fluxes according to Figure 3.21 is reduced with about 20-40% (roughly 0.0006-0.0008 m^3/m^2/year) compared to Case X36. However, strict mathematical comparisons are not meaningful in this context, since not only the gradient differs between the cases, but also the direction of the flow. The latter sometimes implies that an increase of the regional gradient may counteract the local gradient so that the fluxes calculated at a local scale may be reduced although an increased regional gradient has been imposed.

4. Summing Up and Conclusions

Six calculation cases were performed in order to address the model sensitivity to the prevailing regional and local groundwater gradient imposed along the top surface of the modelled domain. The reason for testing this, was an interest in analysing the influence from the imposed gradient on the area around the discharge area (the Imundbo zone), and also to analyse its effect on the recharge area located in the vicinity of the potential repository area.

Two different set-ups were analysed, one with a W–E oriented regional gradient, and one with a SW-NE oriented regional gradient.

By varying the additional W-E gradient, i.e. the one added to the natural one, it was possible to judge the confidence in the discharge area. By imposing a gradient so that the resulting one was three times as high as the natural one, it was found that all the water particles passed through the natural discharge area. The resulting travel times were roughly 40% shorter than for Case X36, and the travel lengths for this situation were also about 40% longer. The case with a resulting total imposed regional gradient roughly twice the natural one, showed that roughly half the number of particles were discharged in the same point as the case described above, whereas the remaining ones were discharged in the Imundbo zone but at a location closer to the repository than for Case X36. The final case for this model set-up, included an additional regional gradient so that the natural one was increased with about 50%. This situation was found to show a somewhat indifferent appearance. All the particles were discharged in the Imundbo zone, but at locations closer to the repository than for Case X36. It was found that the gradient over the discharge area to rather a large extent was counteracted by the imposed gradient, which was the situation for the two former cases. However, since the Imundbo still acted as the discharge area for a case with roughly half the natural gradient, the imposed gradient probably sets some kind of a limit to when the Imundbo can be regarded as the discharge area. This increase (of 0.13%) for the latter case, corresponds to a change in surficial altitude of the groundwater table of about 8 m in the area around the Imundbo zone and roughly 12 m at the west-most model boundary. These values could in some sense be regarded as the uncertainty limit of field measurements, seasonal variations, or any disturbance introduced by man.
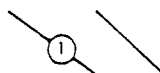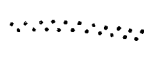
Three calculation cases were analysed with varying degree of disturbance of a topography plane that was fixed along a line parallel to the southern part of the Imundbo zone. One case with an applied regional gradient so that the resulting SW-NE directed local scale gradient was doubled compared to the natural one, indicated that all the particles were discharged in the upper NE corner of the modelled domain. The travel times were reduced with appr. 50% with a simultaneous increase in travel lengths of about 40%, compared to Case X36. A second case with a resulting local gradient reduced by 50% showed a wide spread in discharge locations for the particles. Some of the released particles turned southward directly after them being released, which was found to depend on that they were released in the vicinity of a water divide which was detected now that the gradient was smaller than the natural one. The third case, with an imposed gradient so that the resulting local gradient was about 75% of the natural one, indicated that the particles now approached their natural discharge area, the Imundbo zone. This leads to the conclusion that an applied regional gradient in the order of about 75-100% of the natural one, yields in a discharge at locations that can be regarded as the natural ones. The low end of the span implied that the groundwater table was lowered with about 8-10 m over the potential repository area, with in principle a maintained discharge area. The distribution of pathlines for this set of cases indicated that the imposed gradient to a larger extent coincided with the natural one than was the situation for the cases mentioned above.

Conclusively, one could state that the flow in the repository area is governed by both the local and regional gradient, to a larger extent than the neighbourhood of the discharge area. This depended mainly on that the imposed gradients counteracted the discharge area gradient more than the gradient over the repository area. The gradient in the latter area sometimes interacted with the imposed gradient.
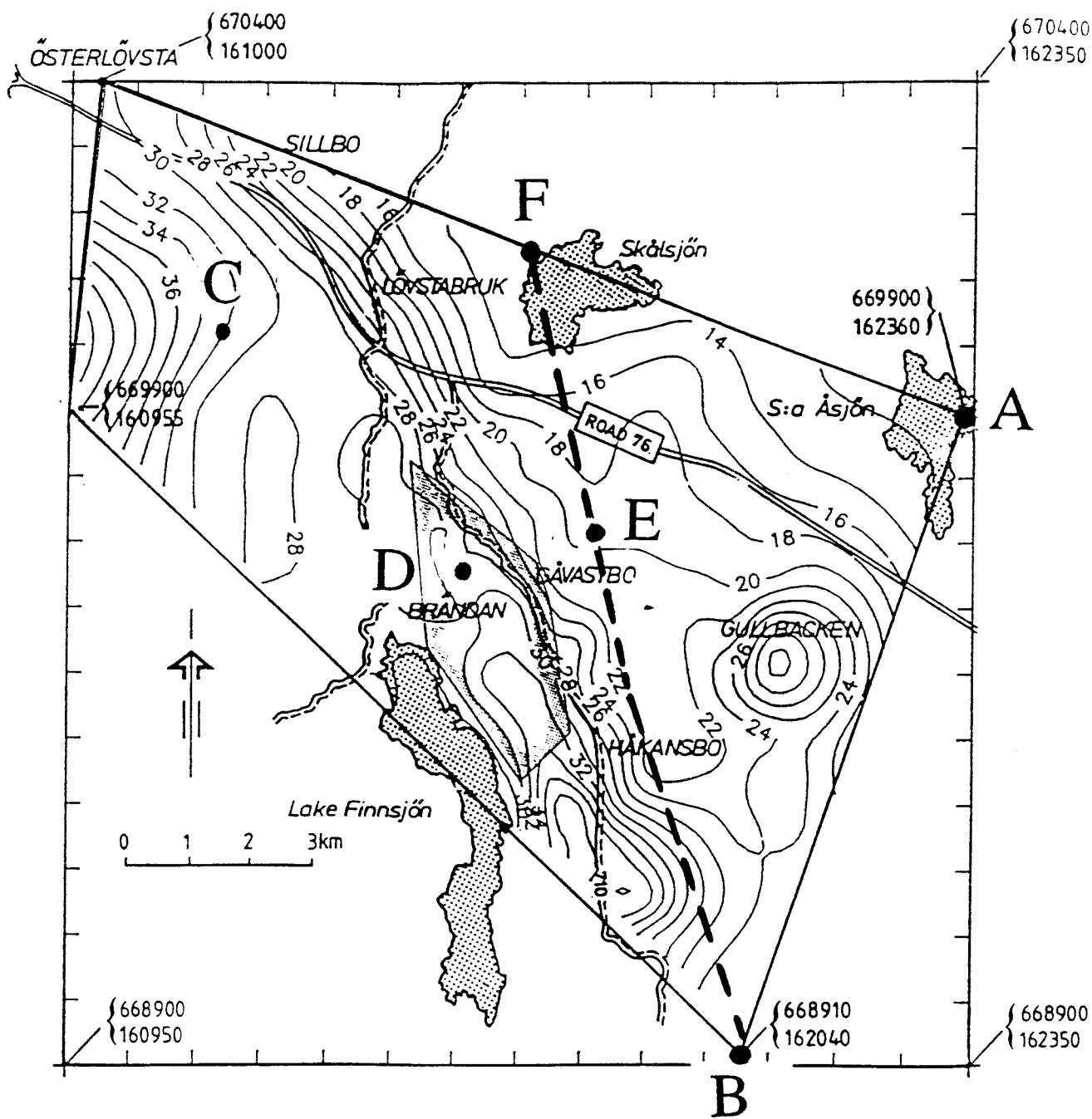
Figures
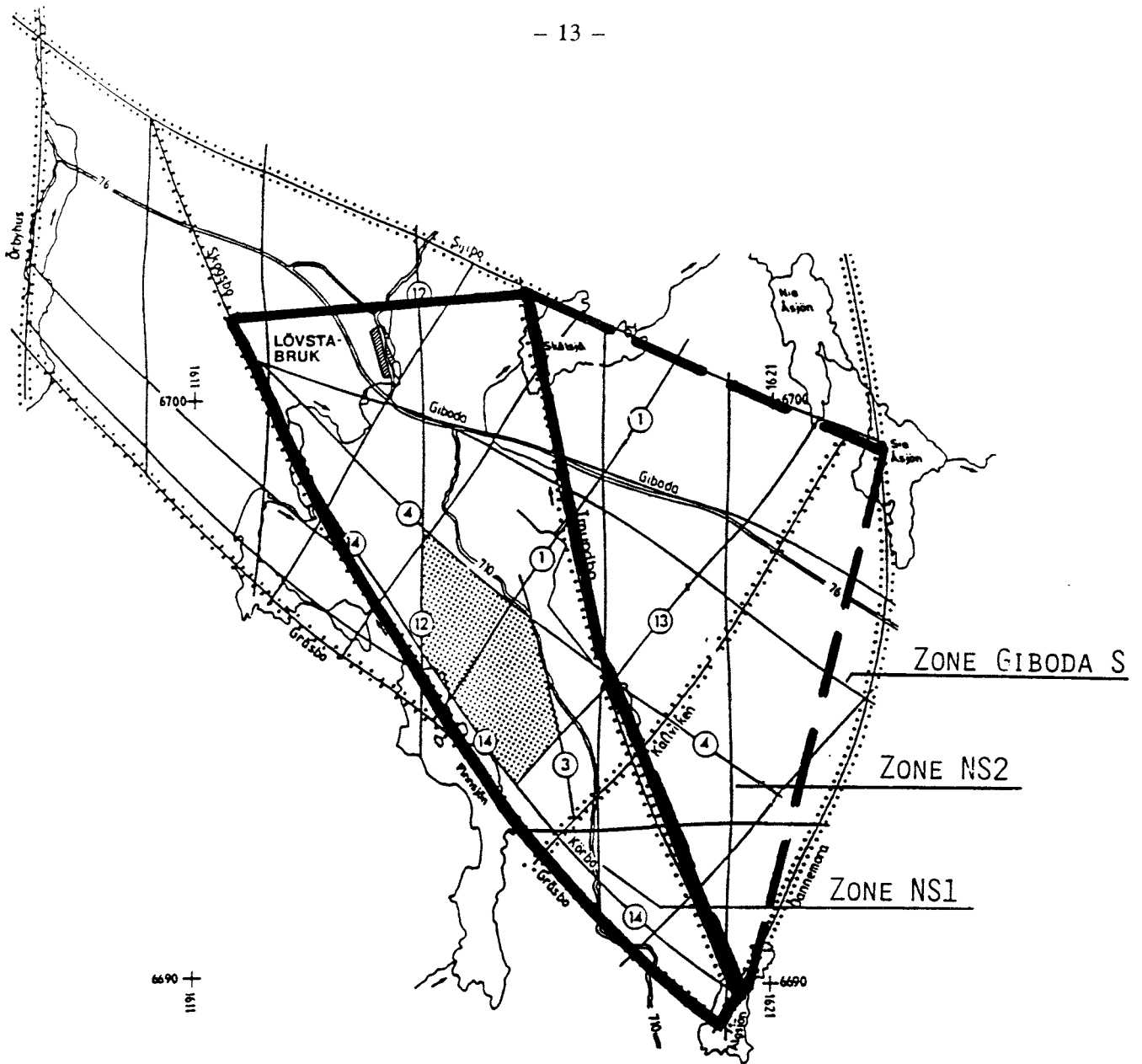
SIMPLIFIED ROCK BLOCK MAP, LÖVSTABRUK AREA

Fracture zones

Position of lineaments interpreted
on regional scale

Finnsjön Rock Block

The glacial striation is north-south

Figure 1.1 *Areal coverage of the semi-regional area as suggested in the SGAB-study (SGAB1, 1991). The area within the solid lines corresponds to that modelled in the KEM2-study, and the area confined by the thick dashed lines corresponds to the extended area as considered within the present study.*
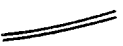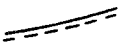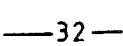
LEGEND:

Road

Minor road

Groundwater ___32___
table contour

Figure 2.1   Topography of the semi-regional area as considered within the present project (from SGAB1, 1991).
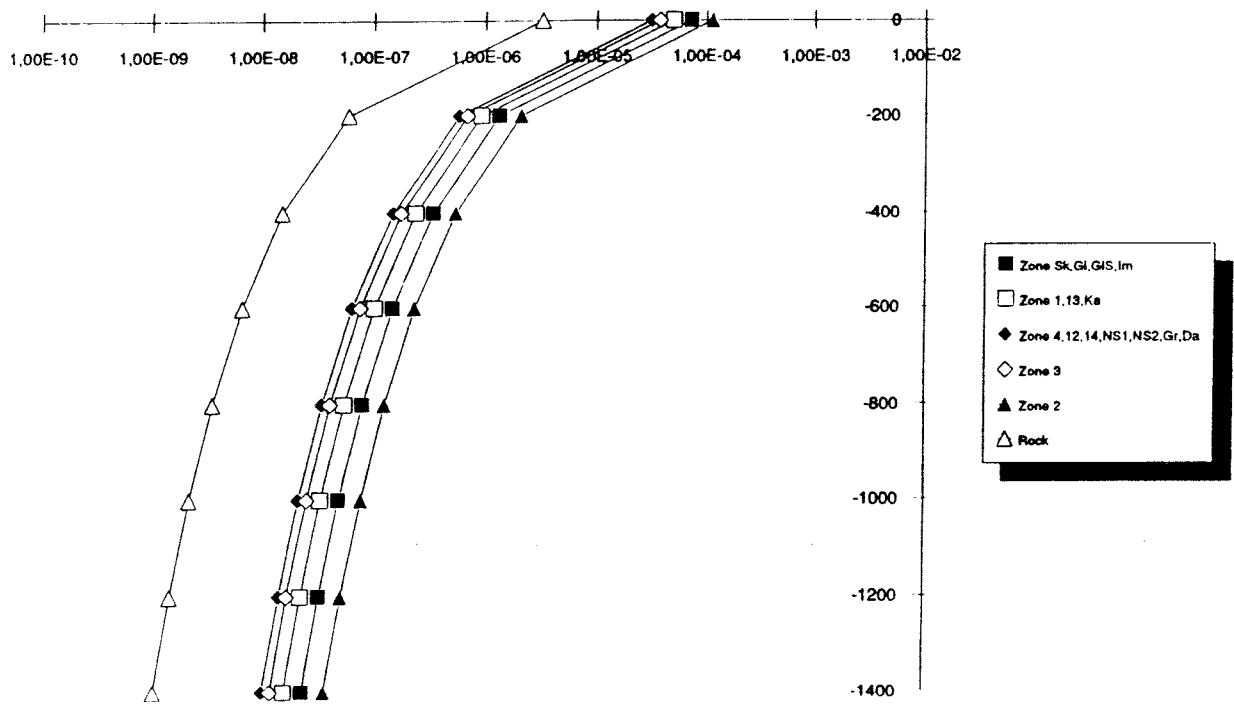
Figure 2.2   Depth dependence of rock mass conductivity and fracture zone conductivities.
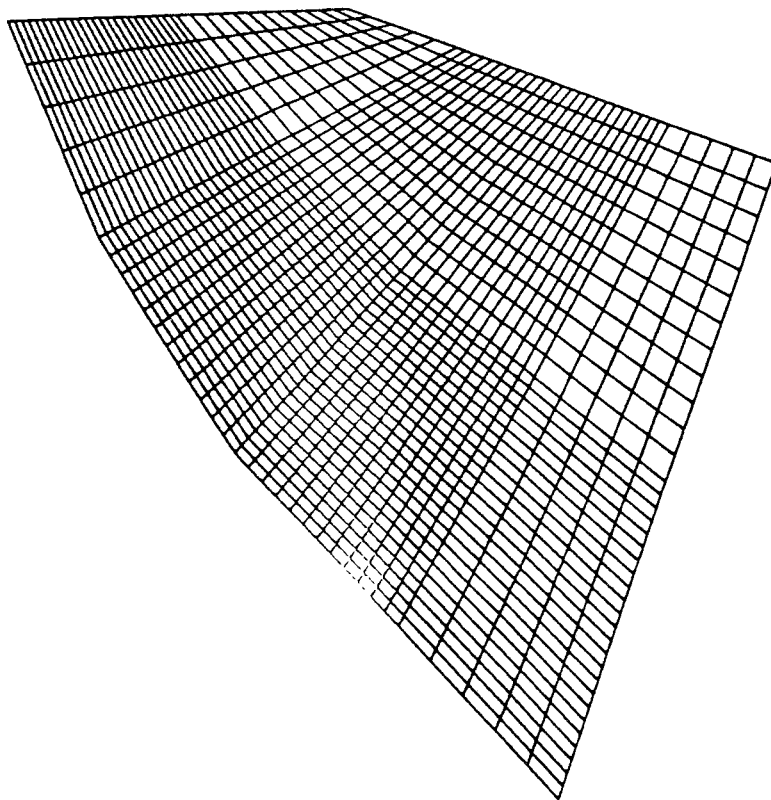
Figure 2.3   Top view of the finite element mesh that was generated.
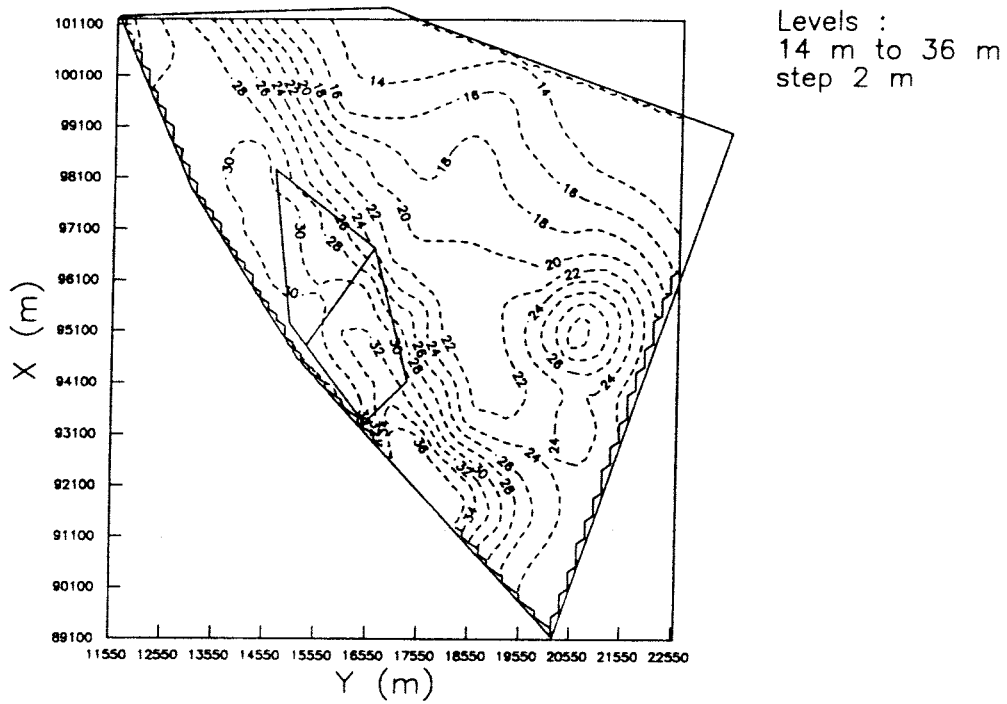
Figure 3.1   *Distribution of hydraulic head at z=0 m for Case X36, see also Figure 2.1.*
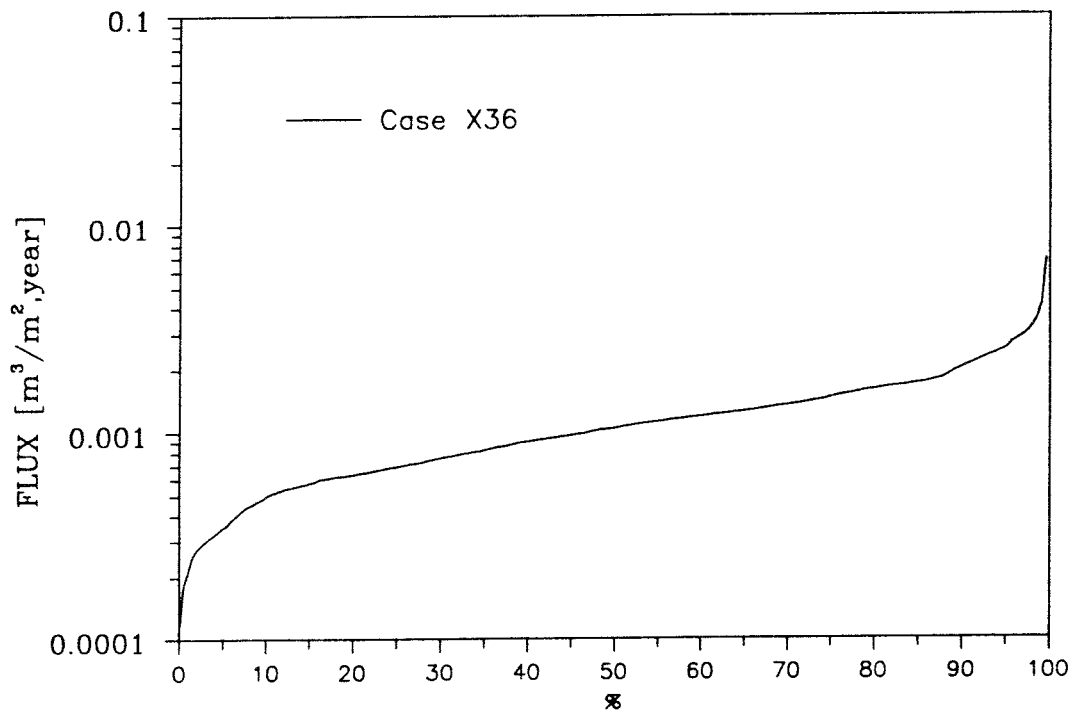
Figure 3.2   *Cumulative flux distribution over repository area for Case X36 (KEM1, 1992).*
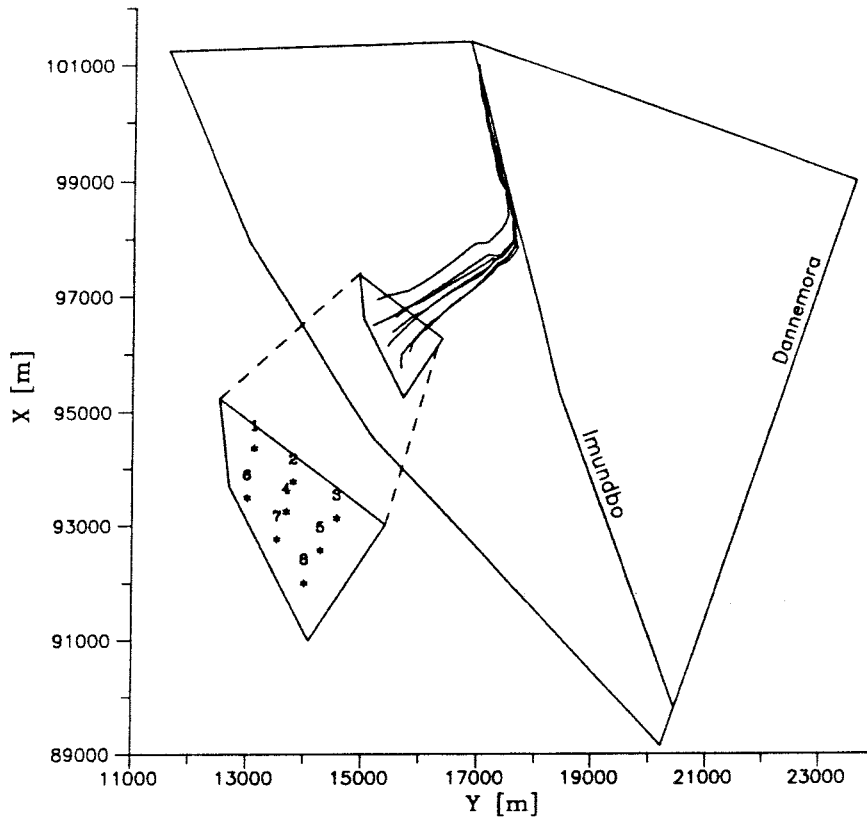
Figure 3.3   Horizontal view of pathlines for Case X36 (KEM1, 1992).

Legend:
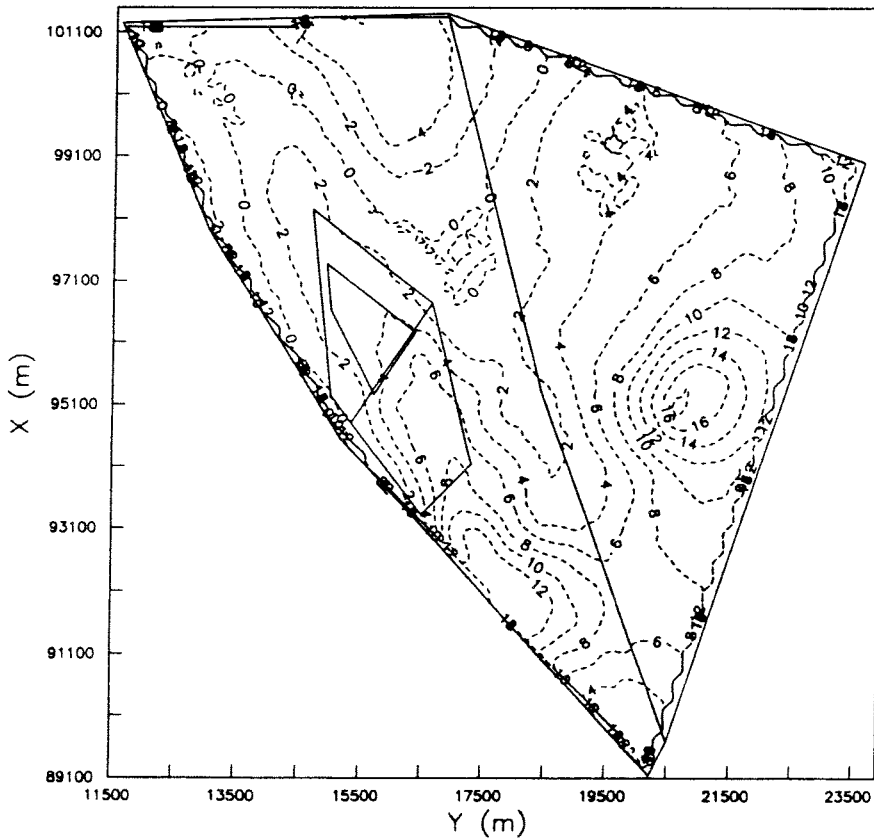
Equidistance 2.0 n

Vertical/horizontal
aspect ratio
1:1
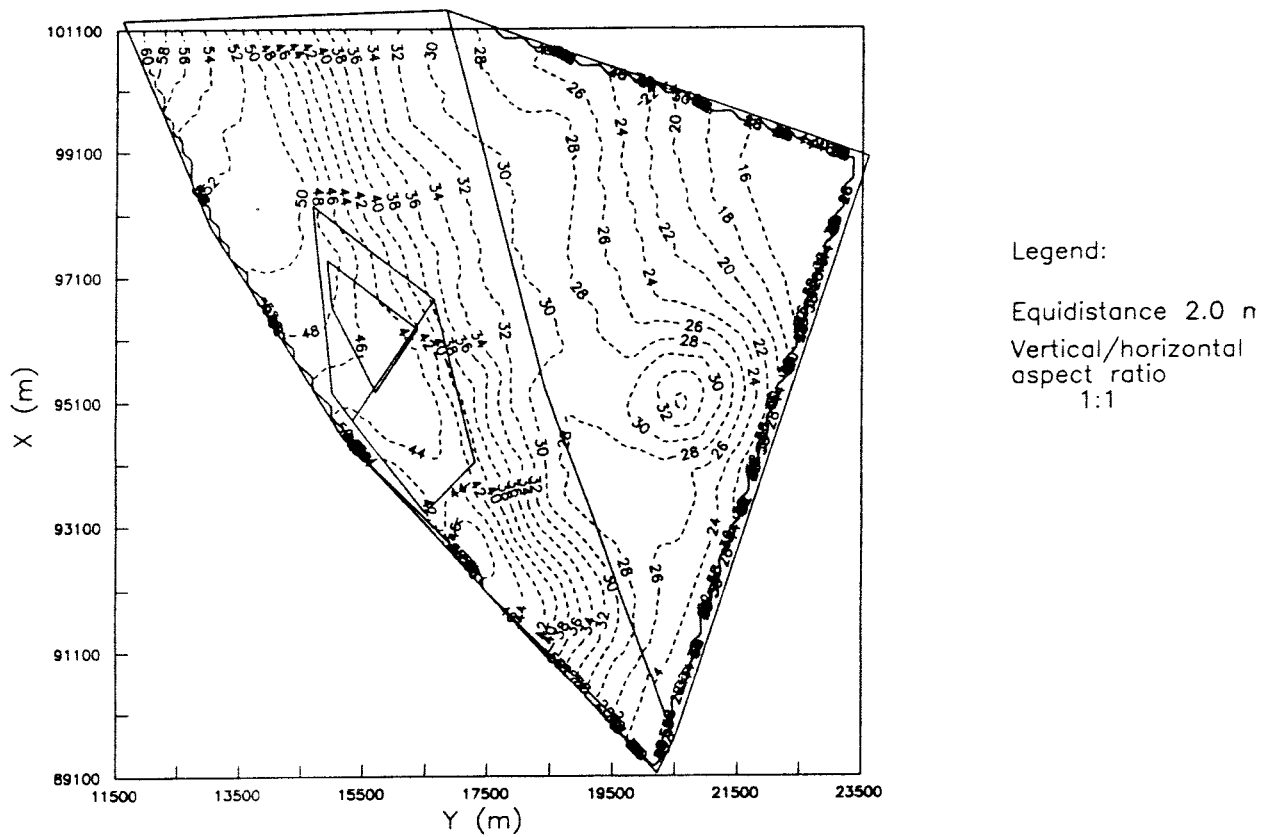
Figure 3.4   Distribution of hydraulic head at z=0 m for Case X36GRV1.
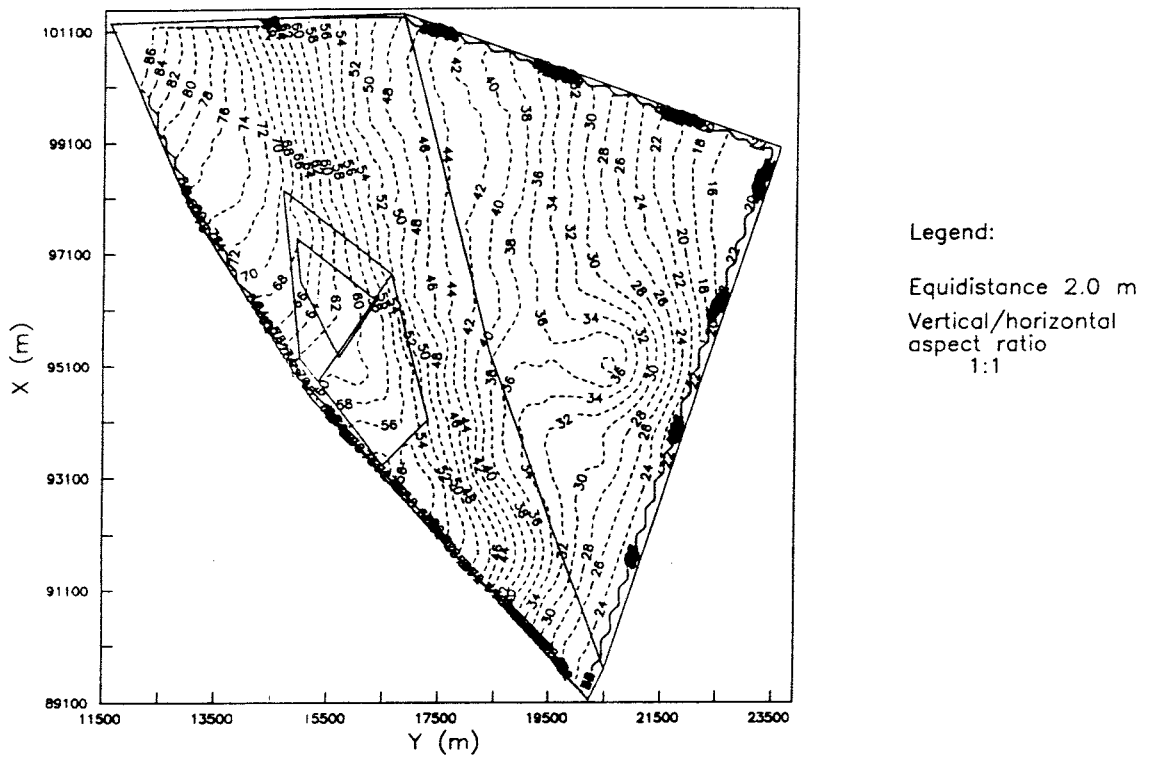
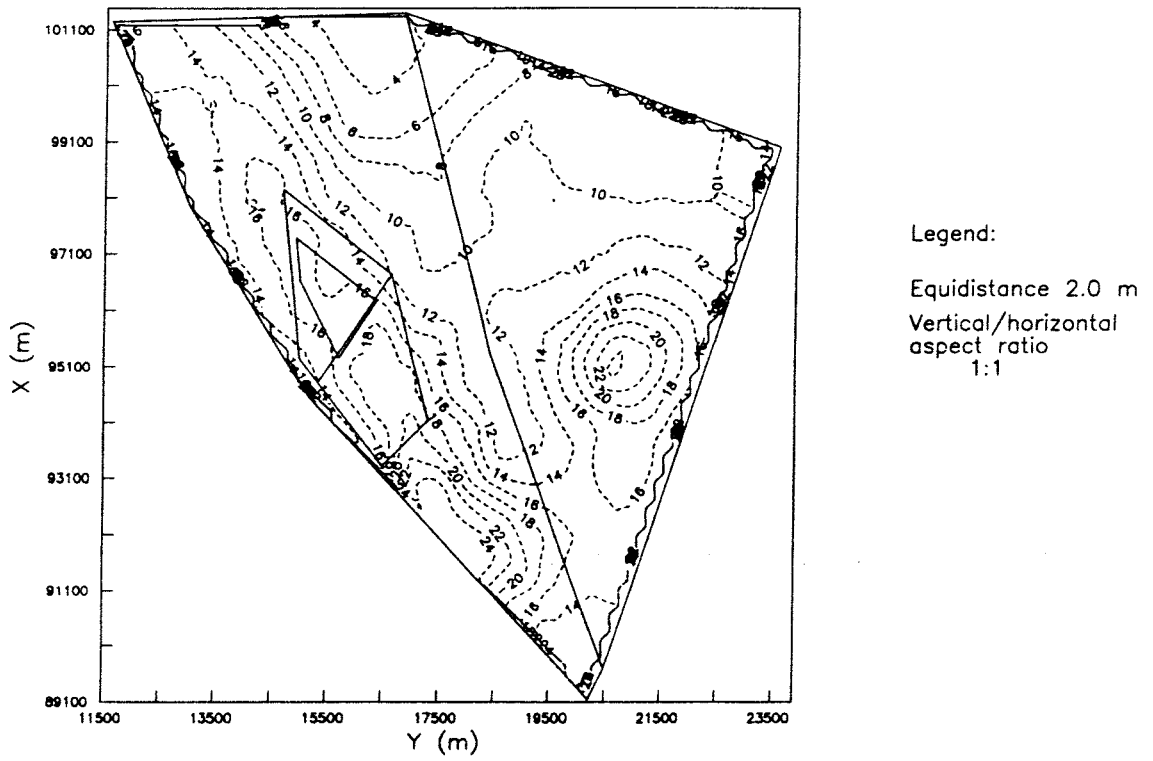*Figure 3.5   Distribution of hydraulic head at z=0 m for Case X36GRV2.*

Legend:

Equidistance 2.0 m

Vertical/horizontal aspect ratio
1:1
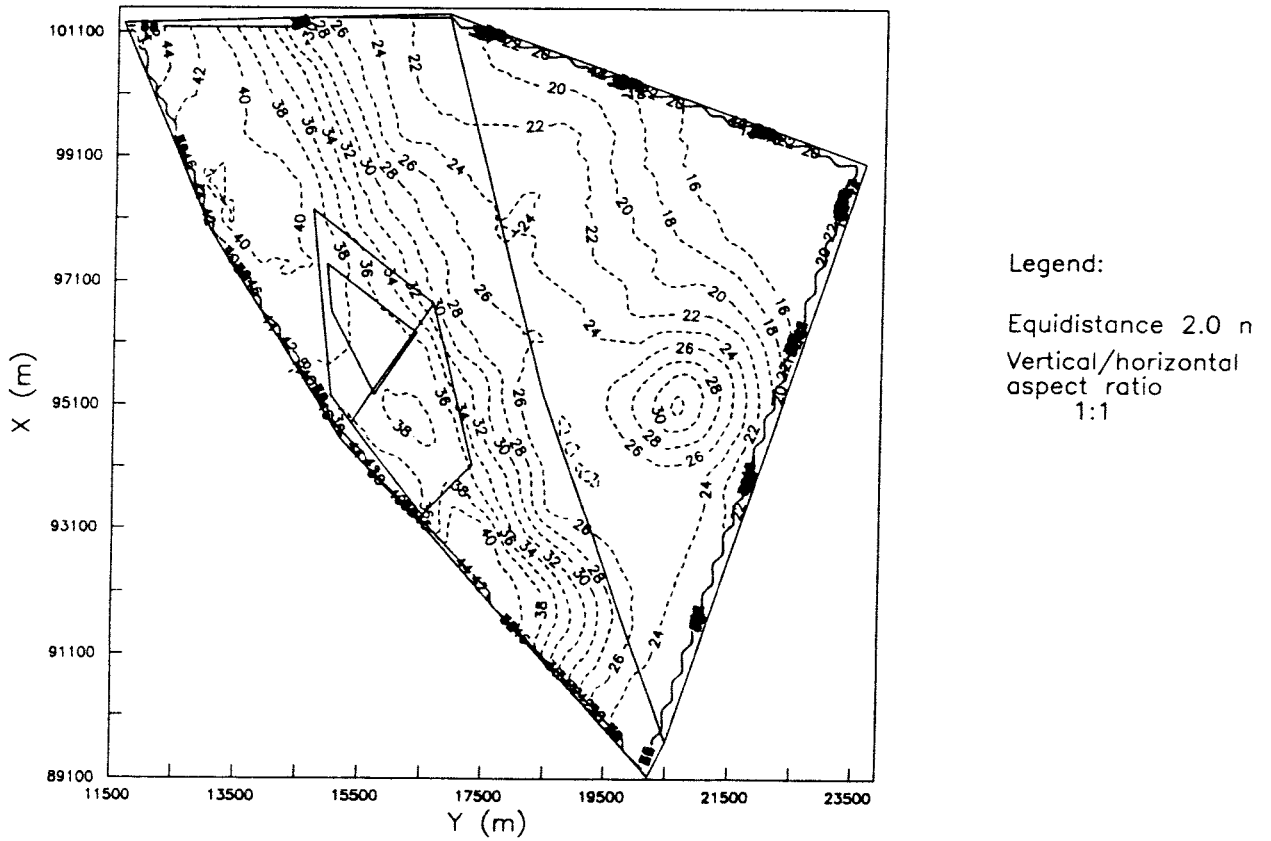
Figure 3.6   Distribution of hydraulic head at z=0 m for Case X36GRV3.

Legend:

Equidistance 2.0 n

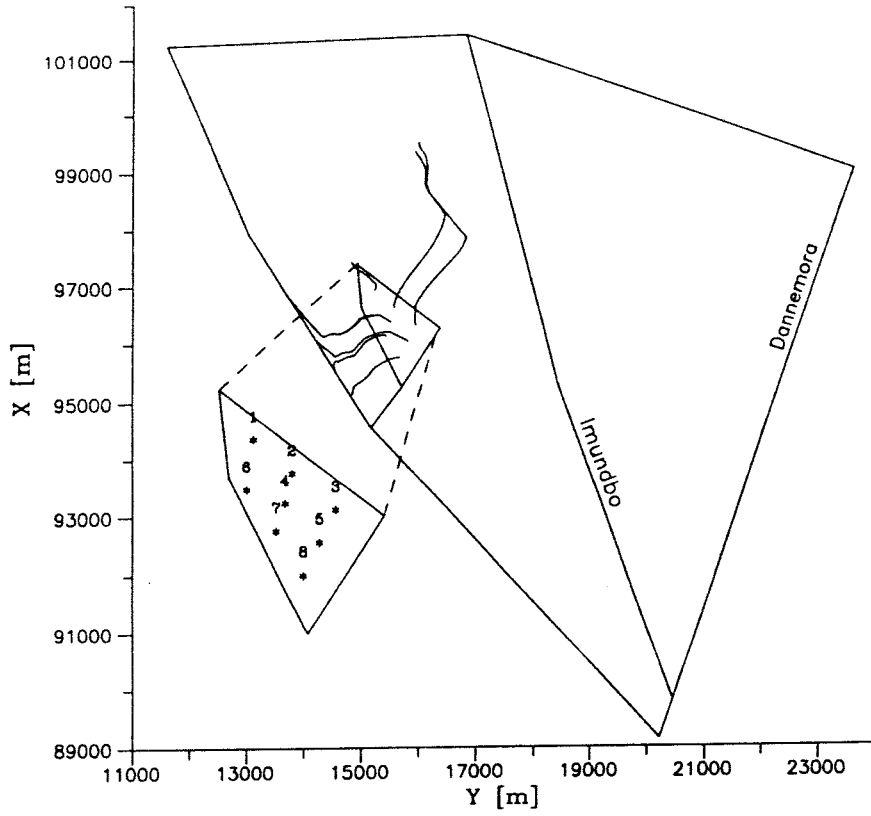Vertical/horizontal aspect ratio
1:1
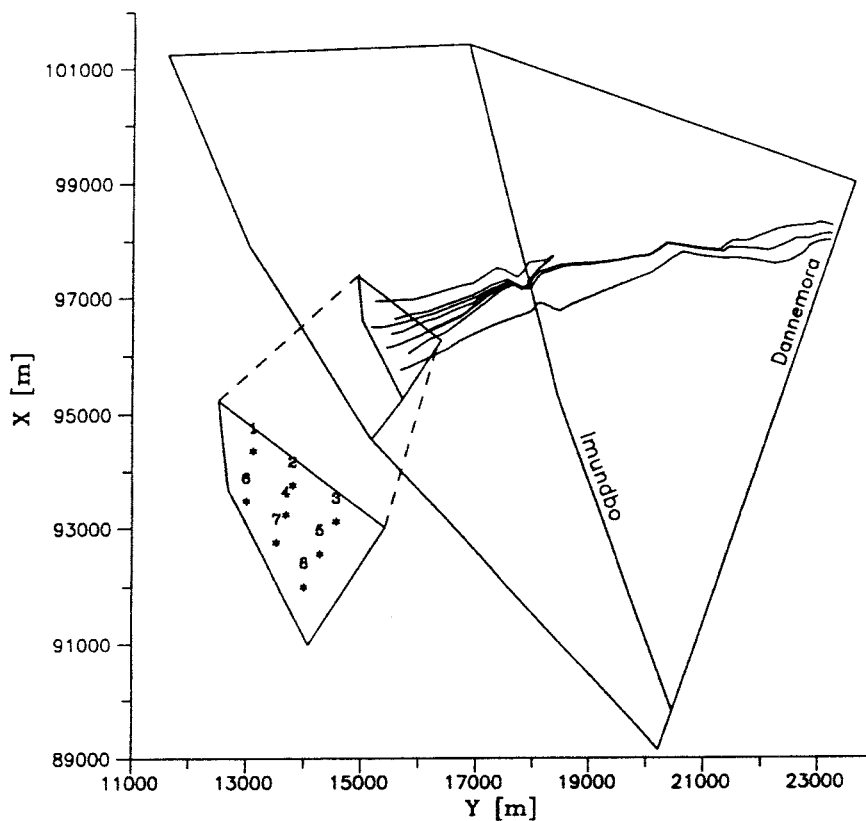
Figure 3.7   *Horizontal projection of pathlines for Case X36GRV1.*
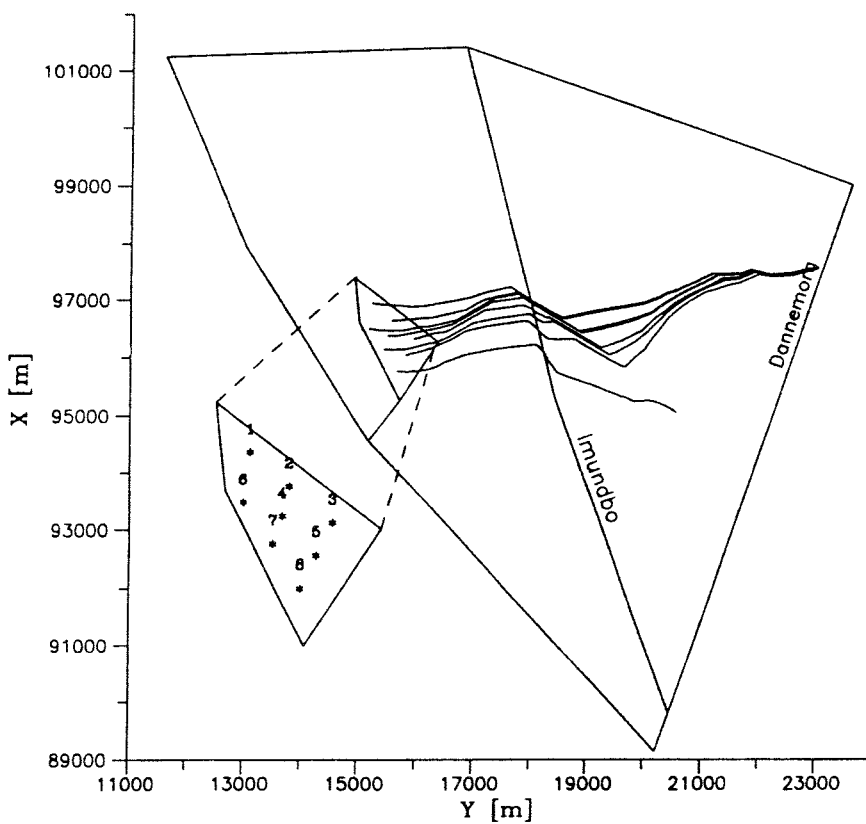
Figure 3.8   *Horizontal projection of pathlines for Case X36GRV2.*
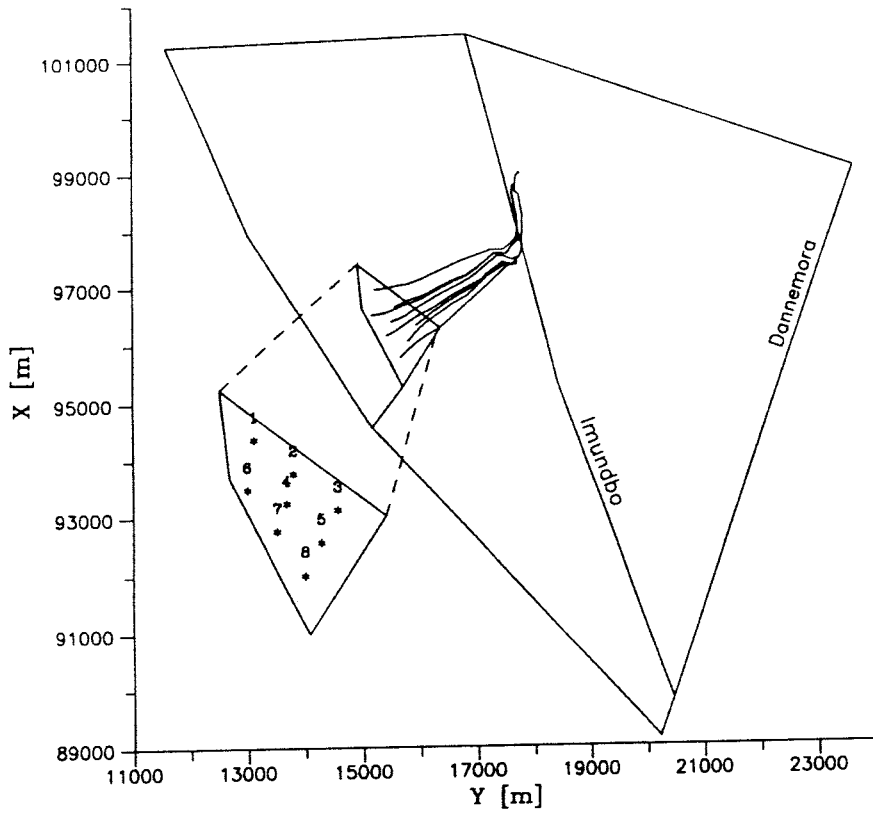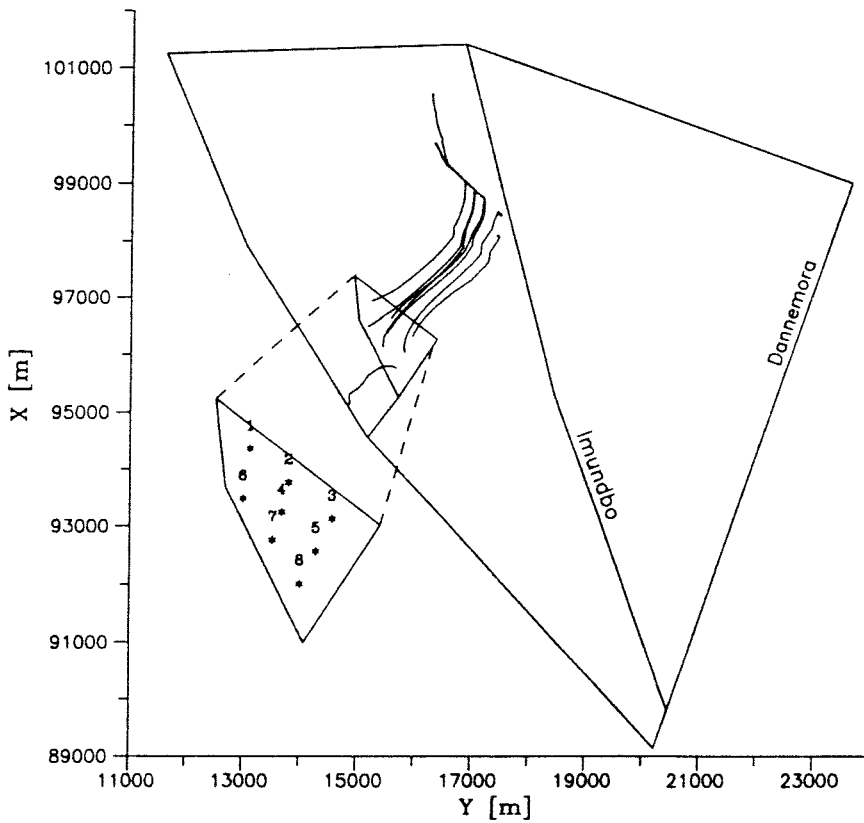
Figure 3.9   *Horizontal projection of pathlines for Case X36GRV3.*
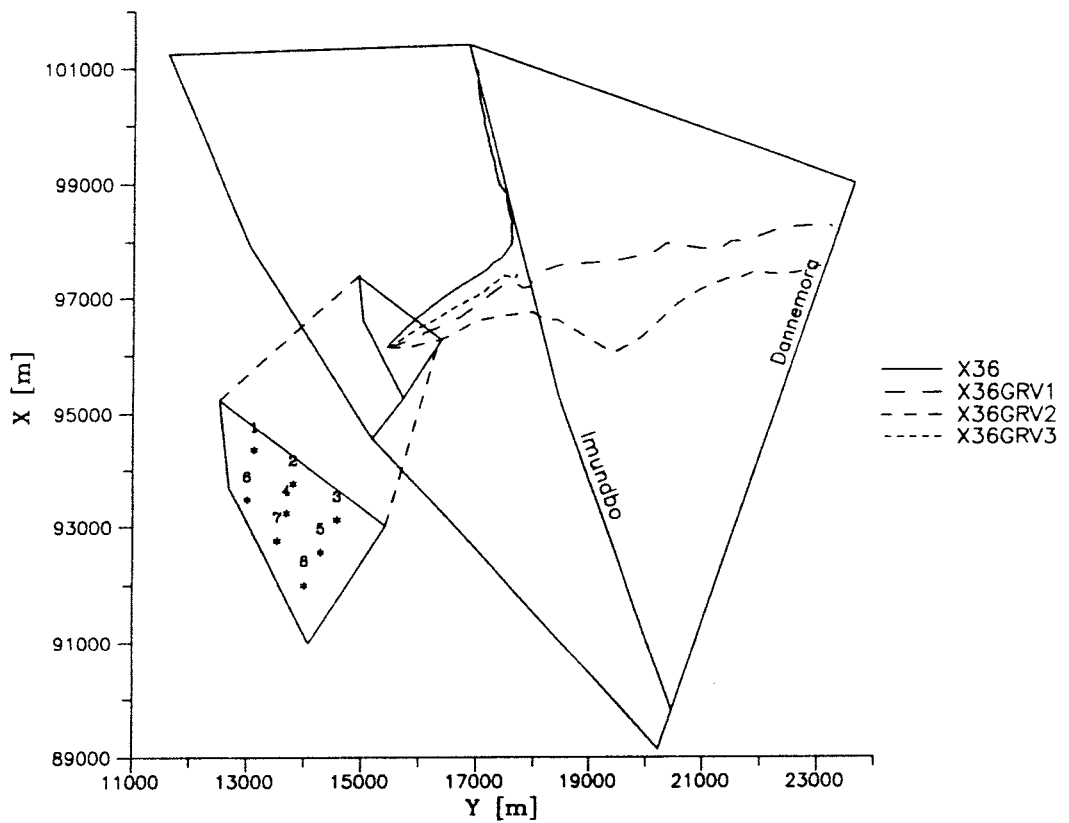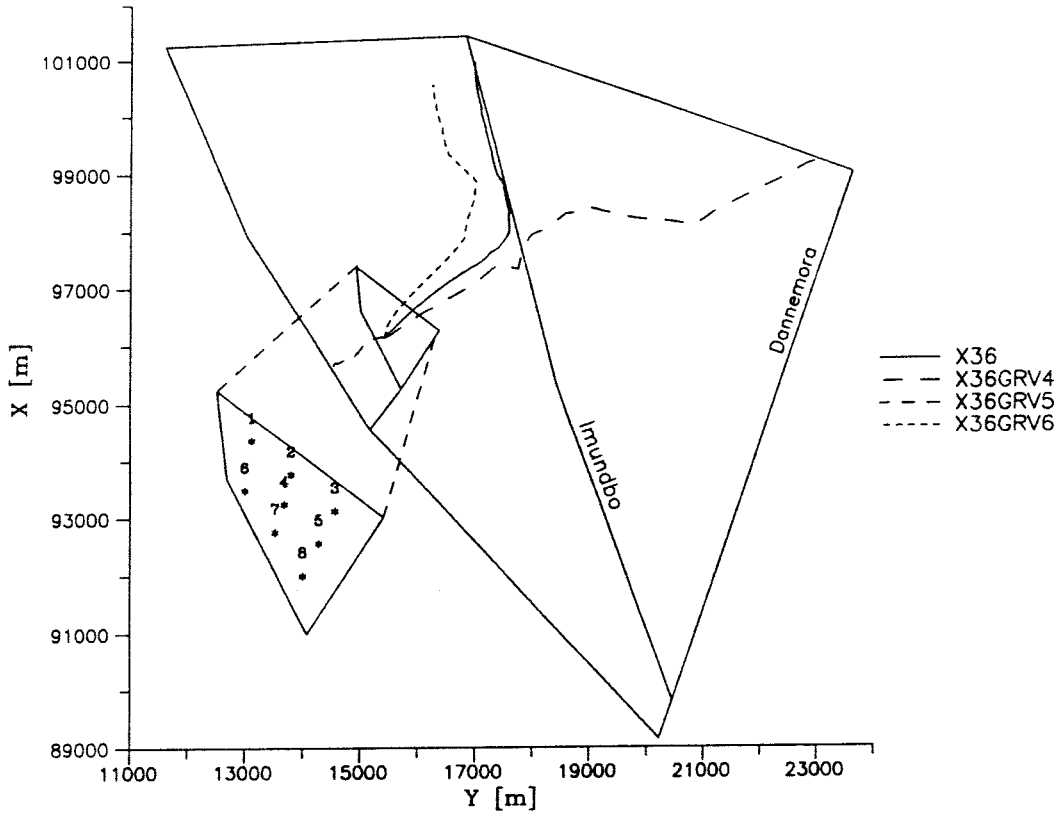

Figure 3.10   *Horizontal projection of flow path 7 for Cases X36GRV1, X36GRV2 and X36GRV3.*
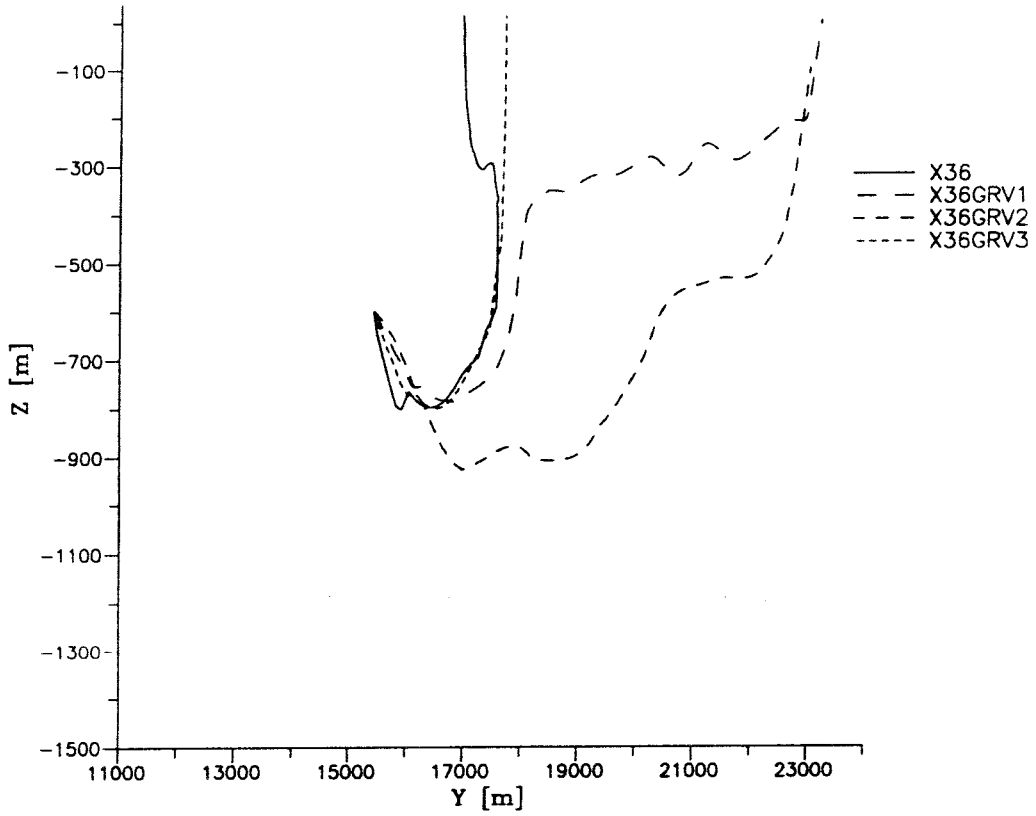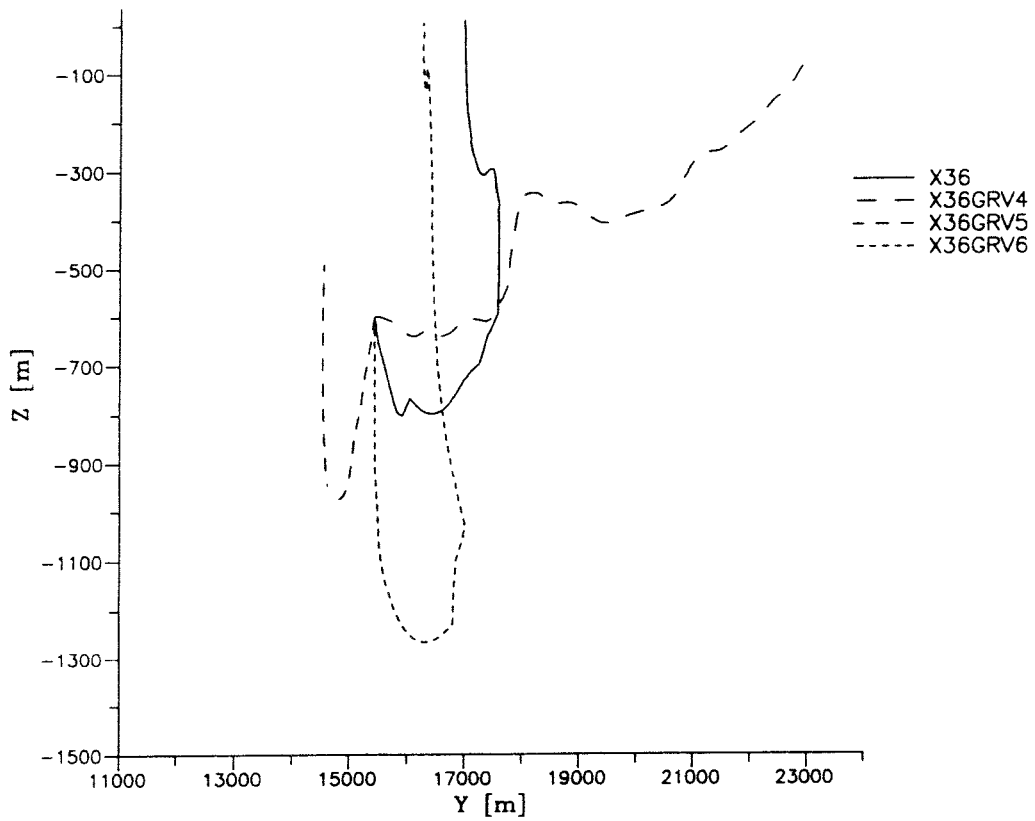
Figure 3.11   Vertical projection (yz-plane) of flow path 7 for Cases X36GRV1, X36GRV2 and X36GRV3.
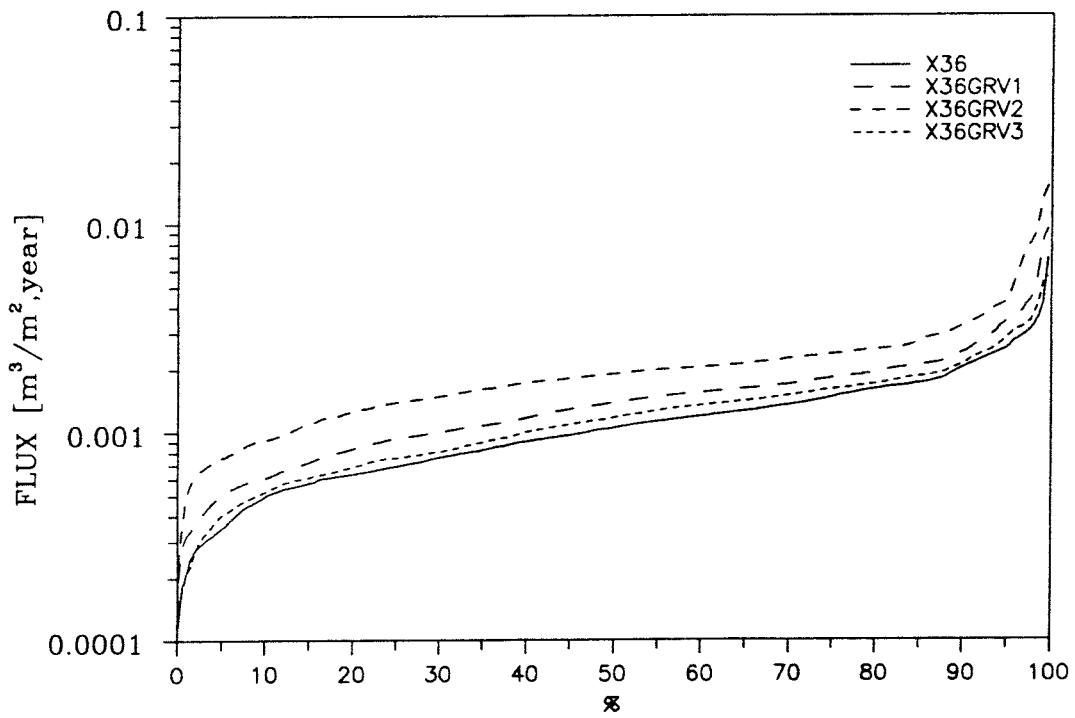
Figure 3.12   Cumulative flux distribution ($m^3/m^2/year$) for Cases X36GRV1, X36GRV2 and X36GRV3 (the results for Case X36 are included for reasons of comparison.
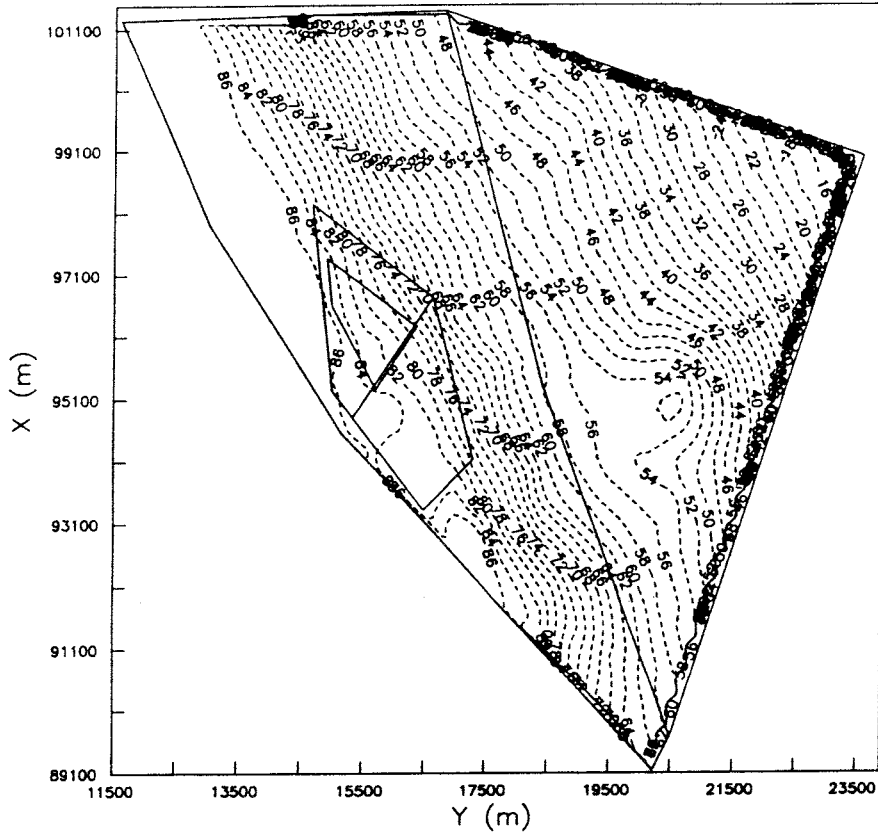
Figure 3.13   Distribution of hydraulic head at z=0 m for Case X36GRV4.

Figure 3.14   Distribution of hydraulic head at z=0 m for Case X36GRV5.

Legend:

Equidistance 2.0 m
Vertical/horizontal
aspect ratio
1:1

Figure 3.15   Distribution of hydraulic head at z=0 m for Case X36GRV6.
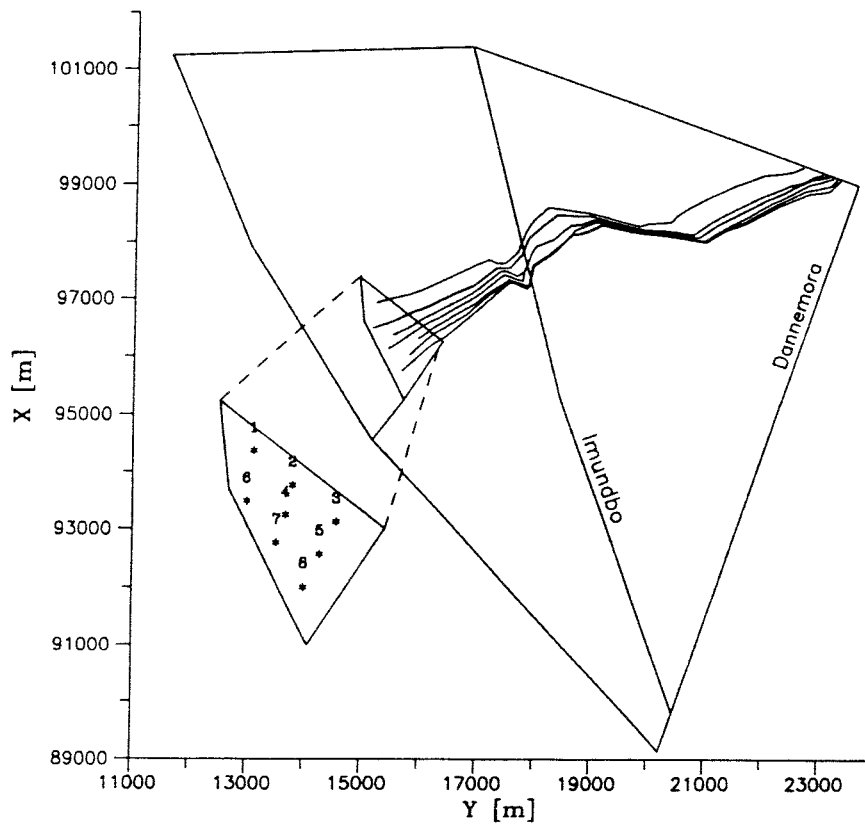
Figure 3.16   Horizontal projection of pathlines for Case X36GRV4.

Figure 3.17   Horizontal projection of pathlines for Case X36GRV5.

Figure 3.18   Horizontal projection of pathlines for Case X36GRV6.

Figure 3.19   *Horizontal projection of flow path 7 for Cases X36GRV4, X36GRV5 and X36GRV6.*

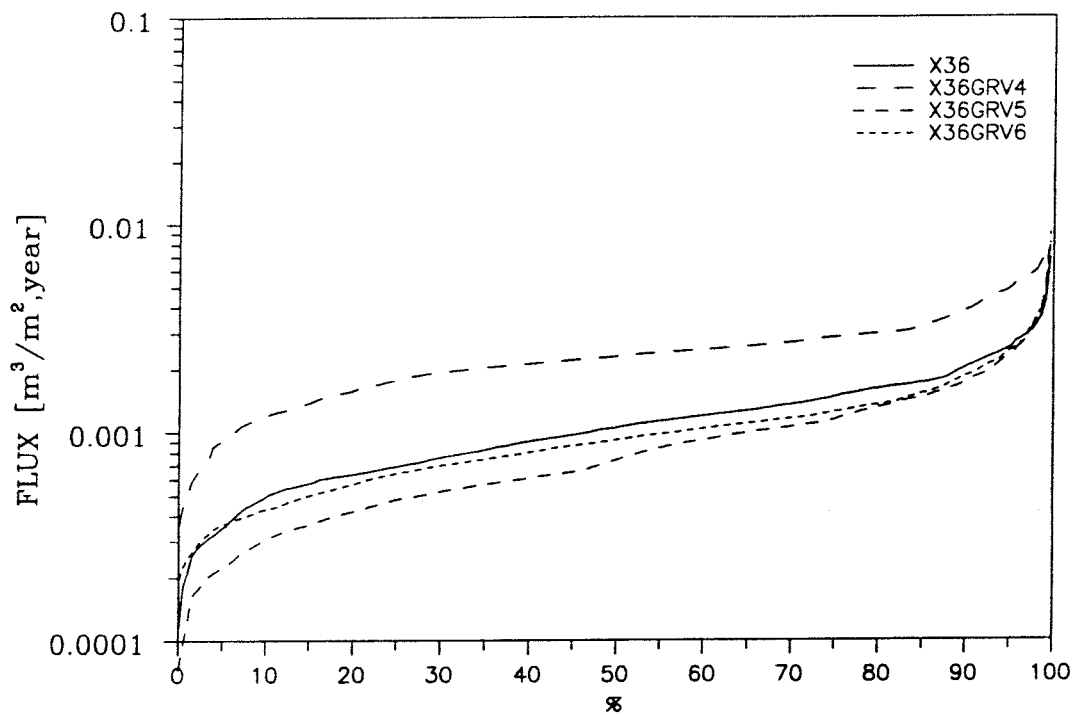*Figure 3.20*   *Vertical projection (yz-plane) of flow path 7 for Cases X36GRV4, X36GRV5 and X36GRV6.*

Figure 3.21   Cumulative flux distribution (m³/m²/year) for Cases X36GRV4, X36GRV5 and
X36GRV6 (the results for Case X36 are included for reasons of comparison.

References

HARW1, 1979:
Rae J., P.C. Robinson, 1979,
"NAMMU: Finite-Element program for coupled heat and groundwater flow problems", Report AERE R-9610, U.K. Atomic Energy Research Establishment, Harwell Laboratory, United Kingdom.

HARW2, 1985:
Atkinson R., A.W. Herbert, C.P. Jackson, P.C. Robinson, 1985,
"NAMMU   User Guide", Report AERE R-11364, U.K. Atomic Energy Research Establishment, Harwell Laboratory, United Kingdom.

KEM1, 1992:
Lindbom B, Boghammar A, 1992,
"Numerical groundwater flow calculations at the Finnsjön study site – extended regional area", SKB Technical Report 92-03, Swedish Nuclear Fuel and Waste Management Company, Stockholm, Sweden.

KEM2, 1991:
Lindbom B, Boghammar A, Lindberg H, Bjelkås J, 1991,
"Numerical groundwater flow calculations at the Finnsjön study site", SKB Technical Report 91-12, Swedish Nuclear Fuel and Waste Management Company, Stockholm, Sweden.

KEM3, 1989:
Grundfelt, B., A. Boghammar, H. Lindberg, 1989
"HYPAC User's Guide", SKB Working Report 89-22, Swedish Nuclear Fuel and Waste Management Company, Stockholm, Sweden.

SGAB1, 1991:
Andersson J-E, Nordqvist R, Nyberg G, Smellie J, Tirén S, 1991,
"Hydrogeological conditions in the Finnsjön area; Compilation of data and conceptual model", SKB Technical Report 91-24, Swedish Nuclear Fuel and Waste Management Company, Stockholm, Sweden.

SGAB2, 1991:
Tirén S, Geosigma AB, Uppsala, Sweden, Personal communication, 1991.

Appendix A

Documentation of files created and processed during the project

For each case the program sequence and input and output files used are listed. The outputfiles marked with a "*" are unique and have been saved. If not otherwhise stated all files reside on /files/home/users/kemhl/0250 on SKB's Convex C220 computer.

For further information with regard to file-name conventions and the contents on the files referred to in this Appendix, see "HYPAC User's Guide", B. Grundfelt, et al, Kemakta Report AR 89-18, Kemakta Consultants Co., Stockholm, Sweden, 1989.

Contents :

CASE F1V5 - X36GRV1

PROPERTY ASSIGNEMENT

BCA :

Input mesh file	=	pre/fixzf119.IFG
Input code file	=	pre/fixz1.OPC
Input BC's file	=	pregr/flv5.itn *
Shell script	=	pregr/dobcaflv5 *
Output mesh file	=	pregr/flv5.BCG

NAMMU AND POSTPROCESSING

NAMMU:

Input mesh file	=	pregr/flv5.BCG
Input perm file	=	pre/fixzf119.IFP
Input nam file	=	nammu/flv5.nam *
Input script-file	=	nammu/donamflv5 *
Output res file	=	nammu/flv5.res * (unformatted)
Output res file	=	nammu/flv5.RES * (formatted)

TRG

Input mesh file	=	pregr/flv5.BCG
Input perm file	=	pre/fixzf119.IFP
Input res file	=	nammu/flv5.RES

Pathlines :		
Shell script	=	postlv5/dobanlv5 *
Output path file(s)	=	postlv5/flv5bB[1-8].DAT
Output path stat	=	postlv5/flv5b.LBN
Horizontal flux projection :		
Shell script	=	postlv5/dotrgflv5 *
Output flux file	=	postlv5/flv5f.DAT
Flux frequency :		
Shell script	=	postlv5/dofprlv5 *
Output freq file	=	postlv5/flv5fq.DAT
Vertical head projection :		
Shell script	=	postlv5/dotrgvlv5 *
Output head file	=	postlv5/flv5v.GRD
Horizontal head projection :		
Shell script	=	postlv5/dotrghlv5 *
Output head file	=	postlv5/flv5h.GRD

CASE F1V6 - X36GRV2

PROPERTY ASSIGNEMENT

BCA :

Input mesh file	=	pre/fixzf119.IFG
Input code file	=	pre/fixz1.OPC
Input BC's file	=	pregr/flv6.itn *
Shell script	=	pregr/dobcaflv6 *
Output mesh file	=	pregr/flv6.BCG

NAMMU AND POSTPROCESSING

NAMMU:

Input mesh file	=	pregr/flv6.BCG
Input perm file	=	pre/fixzf119.IFP
Input nam file	=	nammu/flv6.nam *
Input script-file	=	nammu/donamflv6 *
Output res file	=	nammu/flv6.res * (unformatted)
Output res file	=	nammu/flv6.RES * (formatted)

TRG

Input mesh file	=	pregr/flv6.BCG
Input perm file	=	pre/fixzf119.IFP
Input res file	=	nammu/flv6.RES

Pathlines :
Shell script	=	postlv6/dobanlv6 *
Output path file(s)	=	postlv6/flv6bB[1-8].DAT
Output path stat	=	postlv6/flv6b.LBN

Horizontal flux projection :
Shell script	=	postlv6/dotrgflv6 *
Output flux file	=	postlv6/flv6f.DAT

Flux frequency :
Shell script	=	postlv6/dofprlv6 *
Output freq file	=	postlv6/flv6fq.DAT

Vertical head projection :
Shell script	=	postlv6/dotrgvlv6 *
Output head file	=	postlv6/flv6v.GRD

Horizontal head projection :
Shell script	=	postlv6/dotrghlv6 *
Output head file	=	postlv6/flv6h.GRD

CASE F1V7 - X36GRV3

PROPERTY ASSIGNEMENT

BCA :

Input mesh file	=	pre/fixzf119.IFG
Input code file	=	pre/fixz1.OPC
Input BC's file	=	pregr/flv7.itn *
Shell script	=	pregr/dobcaflv7 *
Output mesh file	=	pregr/flv7.BCG

NAMMU AND POSTPROCESSING

NAMMU:

Input mesh file	=	pregr/flv7.BCG
Input perm file	=	pre/fixzf119.IFP
Input nam file	=	nammu/flv7.nam *
Input script-file	=	nammu/donamflv7 *
Output res file	=	nammu/flv7.res * (unformatted)
Output res file	=	nammu/flv7.RES * (formatted)

TRG

Input mesh file	=	pregr/flv7.BCG
Input perm file	=	pre/fixzf119.IFP
Input res file	=	nammu/flv7.RES

Pathlines :
Shell script	=	postlv7/dobanlv7 *
Output path file(s)	=	postlv7/flv7bB[1-8].DAT
Output path stat	=	postlv7/flv7b.LBN

Horizontal flux projection :
Shell script	=	postlv7/dotrgflv7 *
Output flux file	=	postlv7/flv7f.DAT

Flux frequency :
Shell script	=	postlv7/dofprlv7 *
Output freq file	=	postlv7/flv7fq.DAT

Vertical head projection :
Shell script	=	postlv7/dotrgvlv7 *
Output head file	=	postlv7/flv7v.GRD

Horizontal head projection :
Shell script	=	postlv7/dotrghlv7 *
Output head file	=	postlv7/flv7h.GRD

CASE F1VA - X36GRV4

PROPERTY ASSIGNEMENT

BCA :

Input mesh file	=	pre/fixzf119.IFG
Input code file	=	pre/fixz1.OPC
Input BC's file	=	pregr/f1va.itn *
Shell script	=	pregr/dobcaf1va *
Output mesh file	=	pregr/f1va.BCG

NAMMU AND POSTPROCESSING

NAMMU:

Input mesh file	=	pregr/f1va.BCG
Input perm file	=	pre/fixzf119.IFP
Input nam file	=	nammu/f1va.nam *
Input script-file	=	nammu/donamf1va *
Output res file	=	nammu/f1va.res * (unformatted)
Output res file	=	nammu/f1va.RES * (formatted)

TRG

Input mesh file	=	pregr/f1va.BCG
Input perm file	=	pre/fixzf119.IFP
Input res file	=	nammu/f1va.RES

Pathlines :		
Shell script	=	post1va/doban1va *
Output path file(s)	=	post1va/f1vabB[1-8].DAT
Output path stat	=	post1va/f1vab.LBN
Horizontal flux projection :		
Shell script	=	post1va/dotrgf1va *
Output flux file	=	post1va/f1vaf.DAT
Flux frequency :		
Shell script	=	post1va/dofpr1va *
Output freq file	=	post1va/f1vafq.DAT
Vertical head projection :		
Shell script	=	post1va/dotrgv1va *
Output head file	=	post1va/f1vav.GRD
Horizontal head projection :		
Shell script	=	post1va/dotrgh1va *
Output head file	=	post1va/f1vah.GRD

CASE F1VB - X36GRV5

PROPERTY ASSIGNEMENT

BCA :

Input mesh file	=	pre/fixzf119.IFG
Input code file	=	pre/fixz1.OPC
Input BC's file	=	pregr/f1vb.itn *
Shell script	=	pregr/dobcaf1vb *
Output mesh file	=	pregr/f1vb.BCG

NAMMU AND POSTPROCESSING

NAMMU:

Input mesh file	=	pregr/f1vb.BCG
Input perm file	=	pre/fixzf119.IFP
Input nam file	=	nammu/f1vb.nam *
Input script-file	=	nammu/donamf1vb *
Output res file	=	nammu/f1vb.res * (unformatted)
Output res file	=	nammu/f1vb.RES * (formatted)

TRG

Input mesh file	=	pregr/flvb.BCG
Input perm file	=	pre/fixzf119.IFP
Input res file	=	nammu/flvb.RES

Pathlines :

Shell script	=	post1vb/doban1vb *
Output path file(s)	=	post1vb/flvbbB[1-8].DAT
Output path stat	=	post1vb/flvbb.LBN

Horizontal flux projection :

Shell script	=	post1vb/dotrgflvb *
Output flux file	=	post1vb/flvbf.DAT

Flux frequency :

Shell script	=	post1vb/dofpr1vb *
Output freq file	=	post1vb/flvbfq.DAT

Vertical head projection :

Shell script	=	post1vb/dotrgvlvb *
Output head file	=	post1vb/flvbv.GRD

Horizontal head projection :

Shell script	=	post1vb/dotrghlvb *
Output head file	=	post1vb/flvbh.GRD

CASE F1VC - X36GRV6

PROPERTY ASSIGNEMENT

BCA :

Input mesh file	=	pre/fixzf119.IFG
Input code file	=	pre/fixz1.OPC
Input BC's file	=	pregr/flvc.itn *
Shell script	=	pregr/dobcaflvc *
Output mesh file	=	pregr/flvc.BCG

NAMMU AND POSTPROCESSING

NAMMU:

Input mesh file	=	pregr/flvc.BCG
Input perm file	=	pre/fixzf119.IFP
Input nam file	=	nammu/flvc.nam *
Input script-file	=	nammu/donamflvc *
Output res file	=	nammu/flvc.res * (unformatted)
Output res file	=	nammu/flvc.RES * (formatted)

TRG

Input mesh file	=	pregr/flvc.BCG
Input perm file	=	pre/fixzf119.IFP
Input res file	=	nammu/flvc.RES

Pathlines :

Shell script	=	post1vc/doban1vc *
Output path file(s)	=	post1vc/flvcbB[1-8].DAT
Output path stat	=	post1vc/flvcb.LBN

Horizontal flux projection :

Shell script	=	post1vc/dotrgflvc *
Output flux file	=	post1vc/flvcf.DAT

Flux frequency :

Shell script	=	post1vc/dofpr1vc *
Output freq file	=	post1vc/flvcfq.DAT

Vertical head projection :

Shell script	=	post1vc/dotrgvlvc *
Output head file	=	post1vc/flvcv.GRD

Horizontal head projection :

Shell script	=	post1vc/dotrghlvc *
Output head file	=	post1vc/flvch.GRD

Appendix B

Evaluation figures not presented in the current text
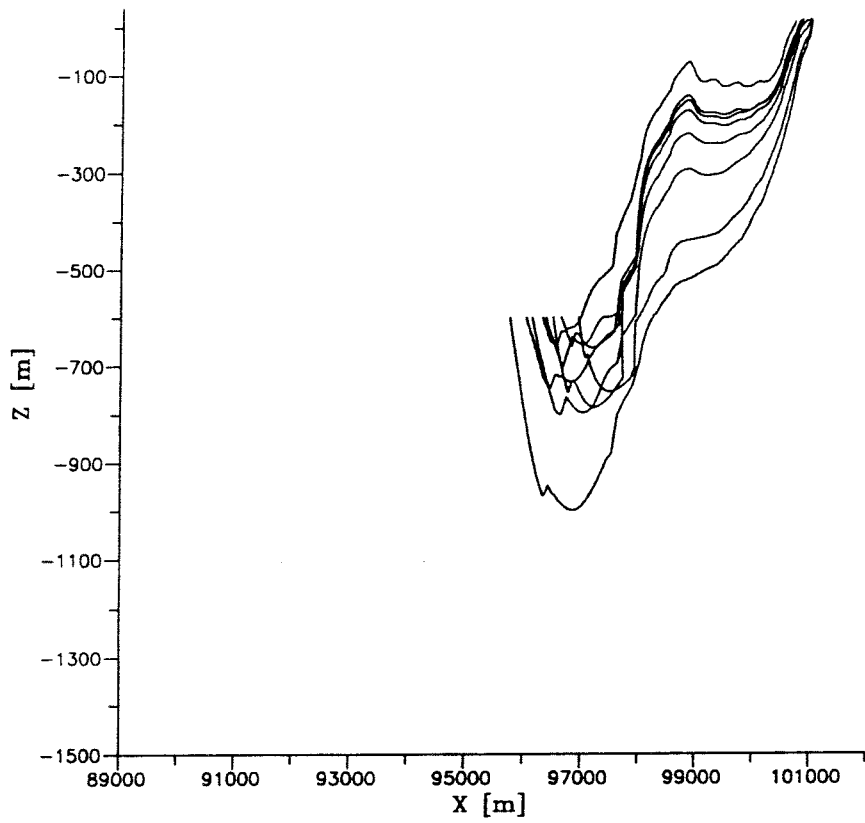
Figure B1   *Vertical view of pathlines (xz-plane) for Case X36 (KEMI, 1992).*
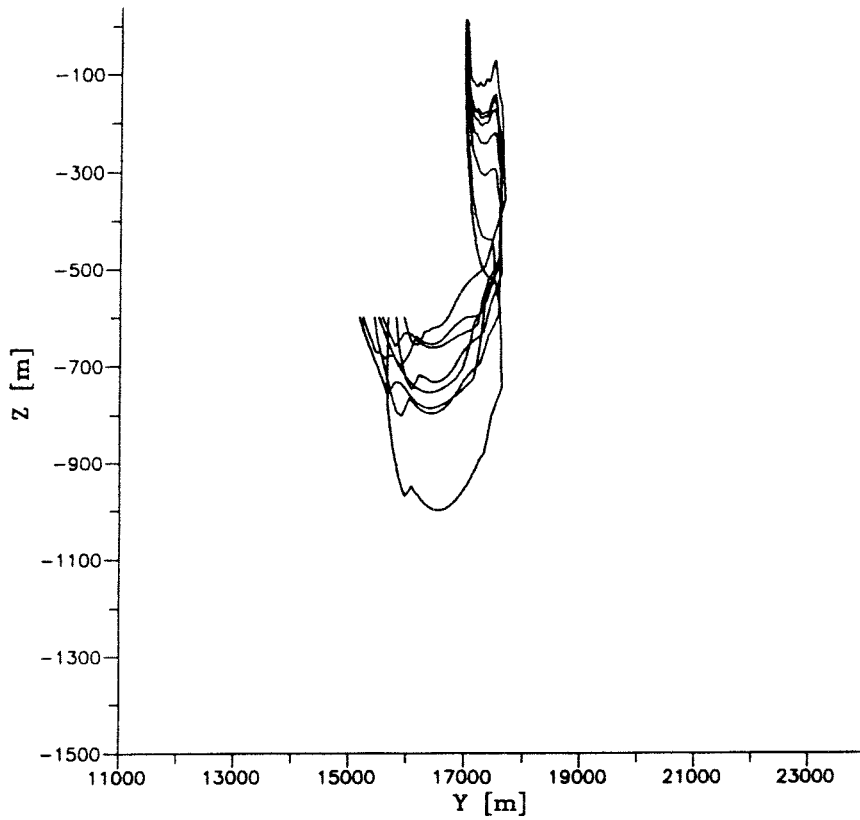
Figure B2   *Vertical view of pathlines (yz-plane) for Case X36 (KEMI, 1992).*
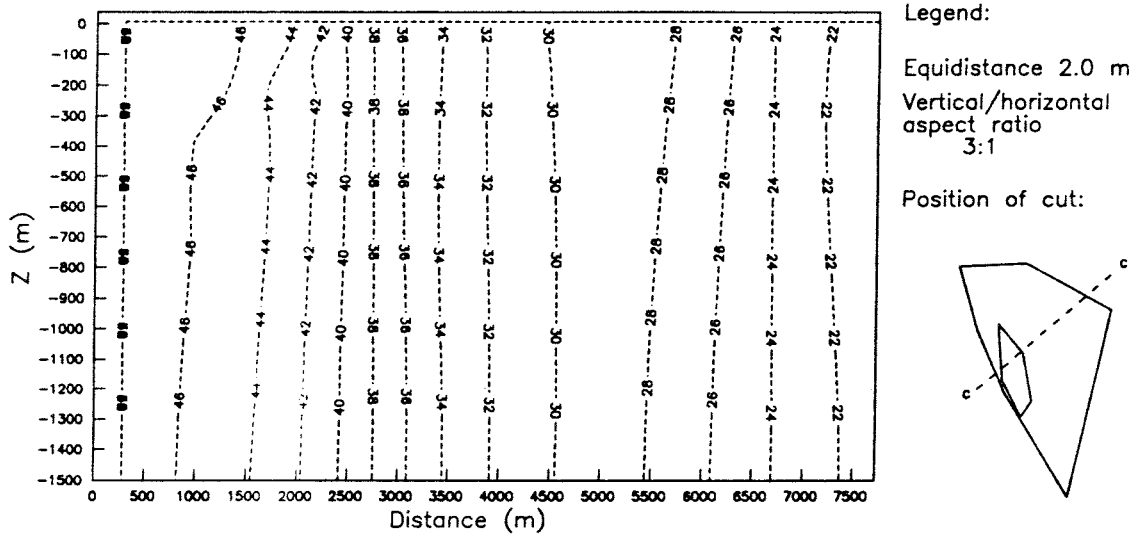
Figure B3   *Distribution of hydraulic head in a vertical cross-section for Case X36GRV1.*
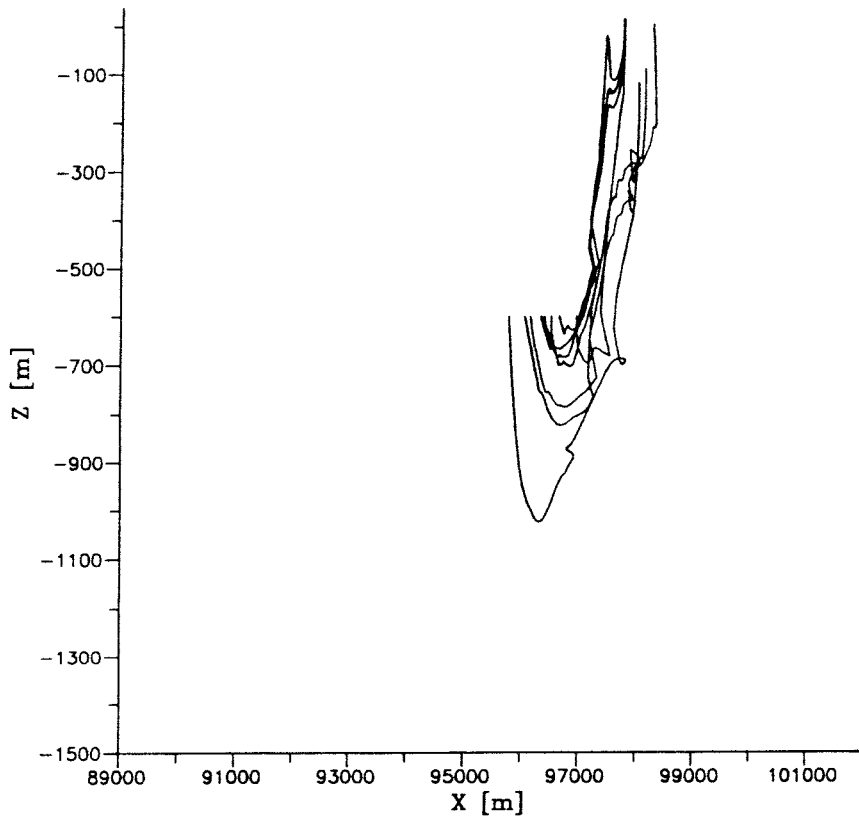
Figure B4   *Vertical projection (xz-plane) of pathlines for Case X36GRV1.*
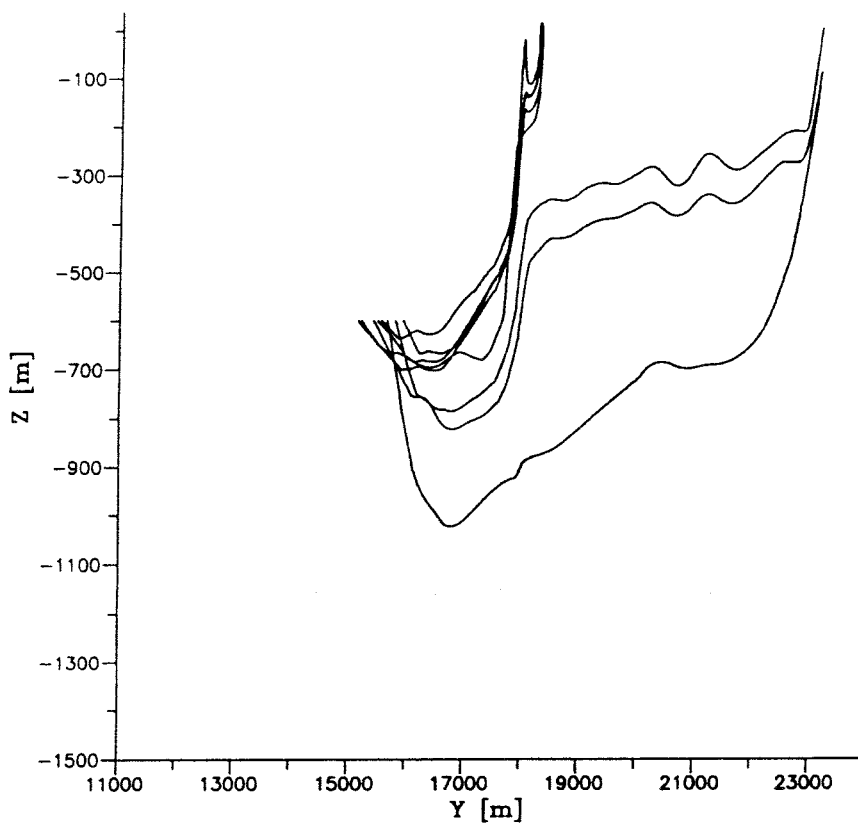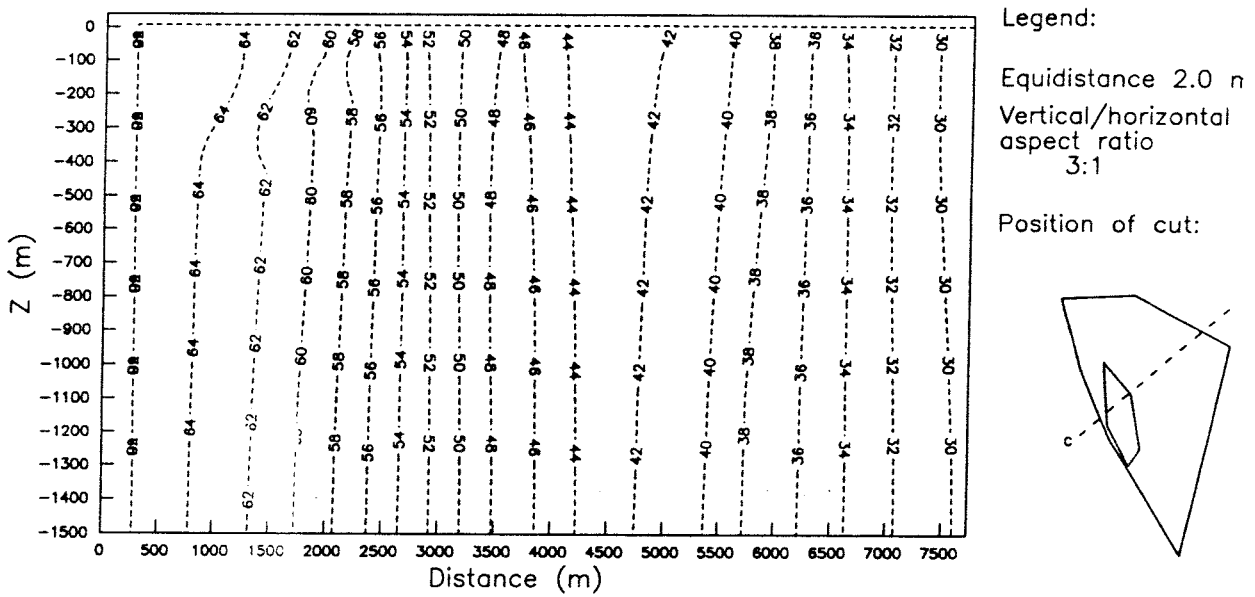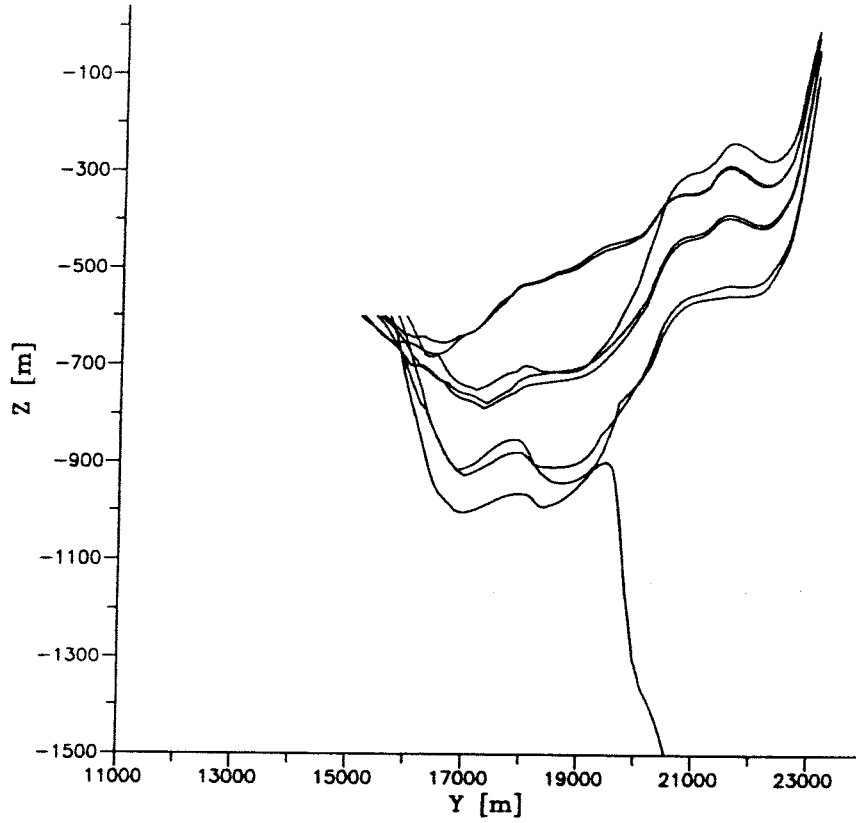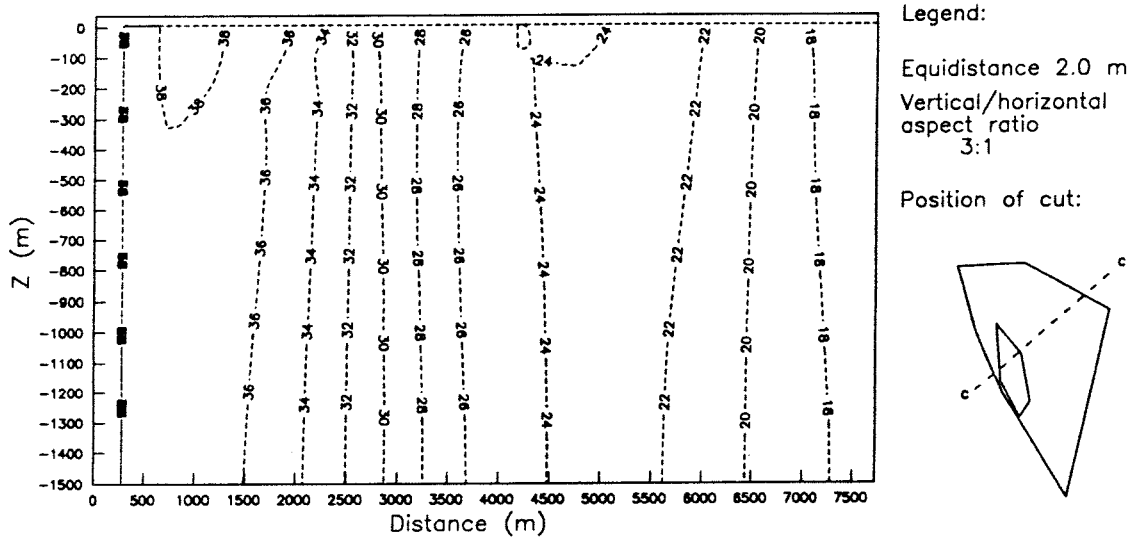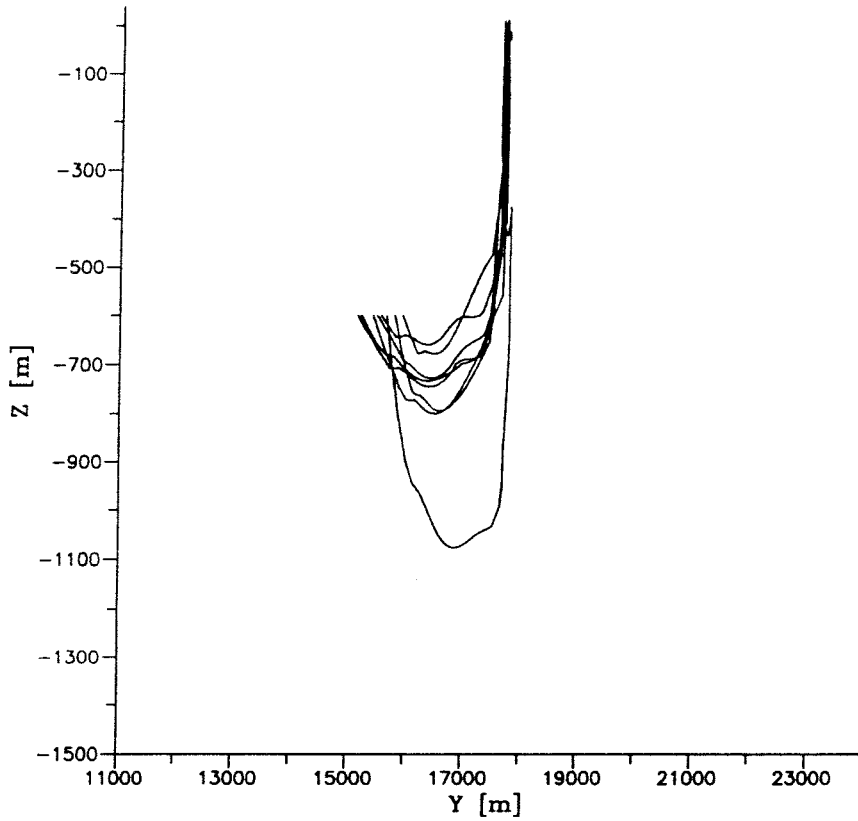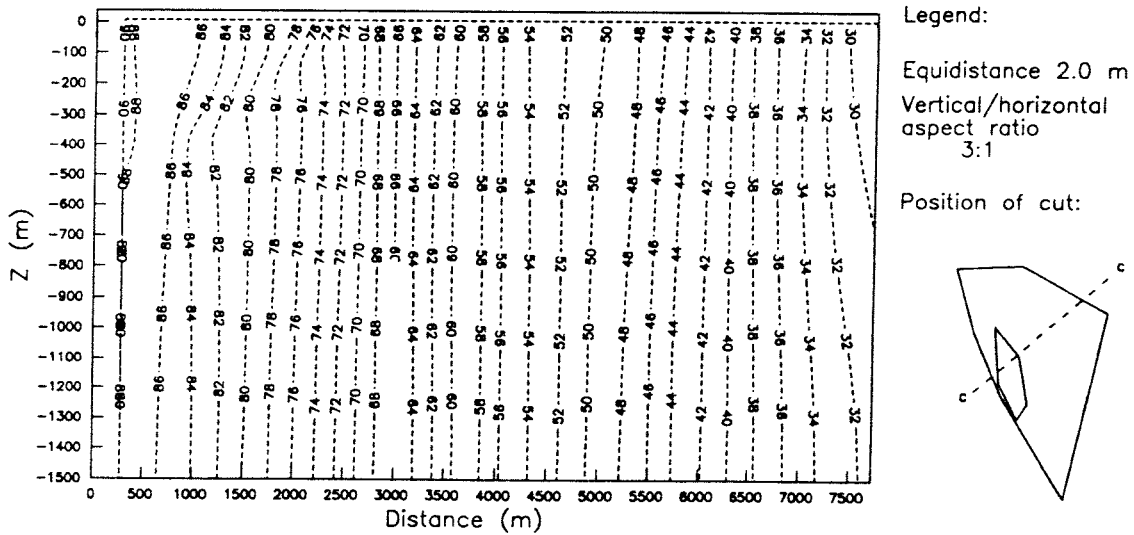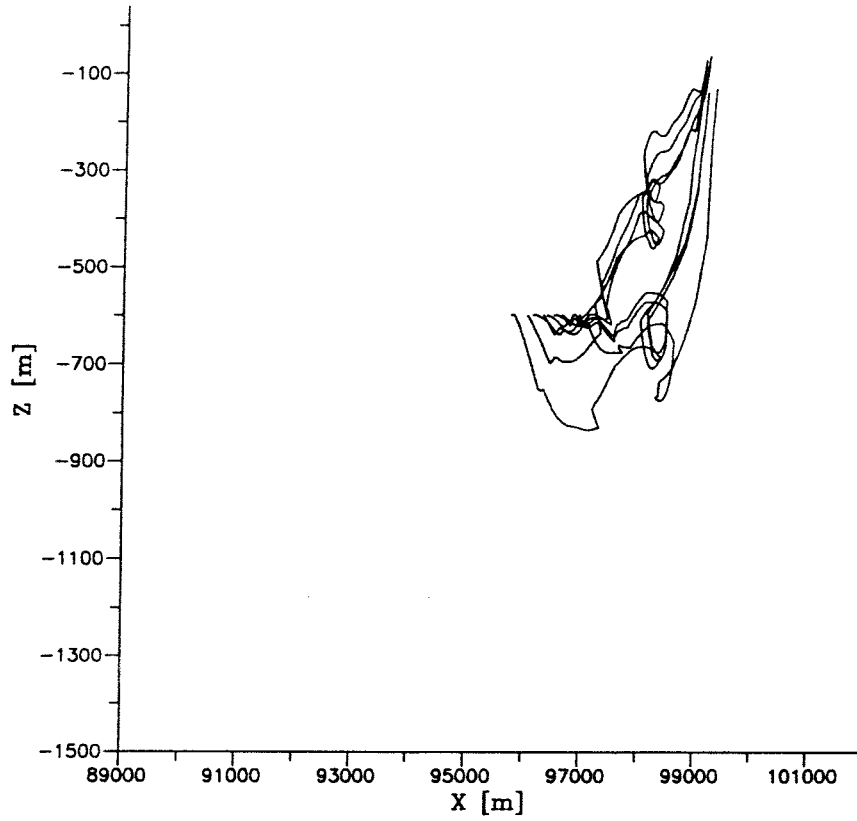
Figure B5　　　*Vertical projection (yz-plane) of pathlines for Case X36GRV1.*
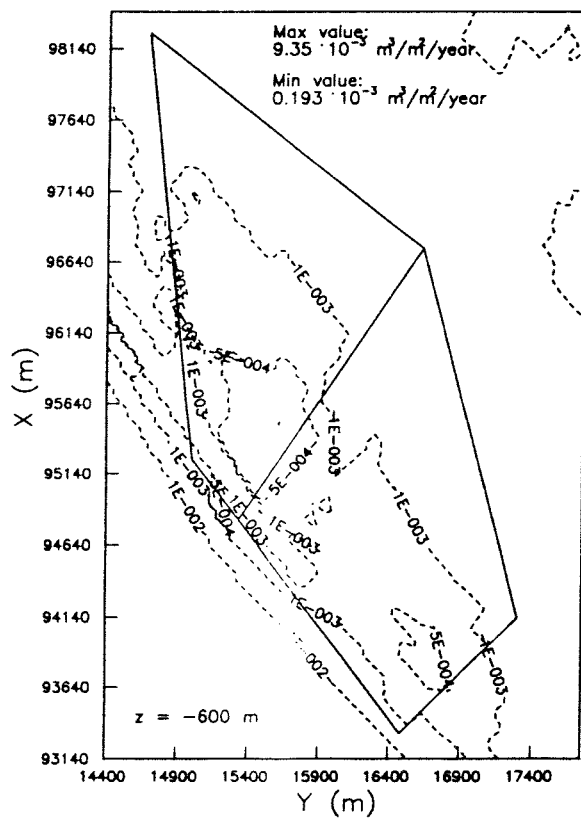
Figure B6　　　*Contoured flux distribution (m³/m²/year) for Case X36GRV1.*

Figure B7   *Distribution of hydraulic head in a vertical cross-section for Case X36GRV2.*
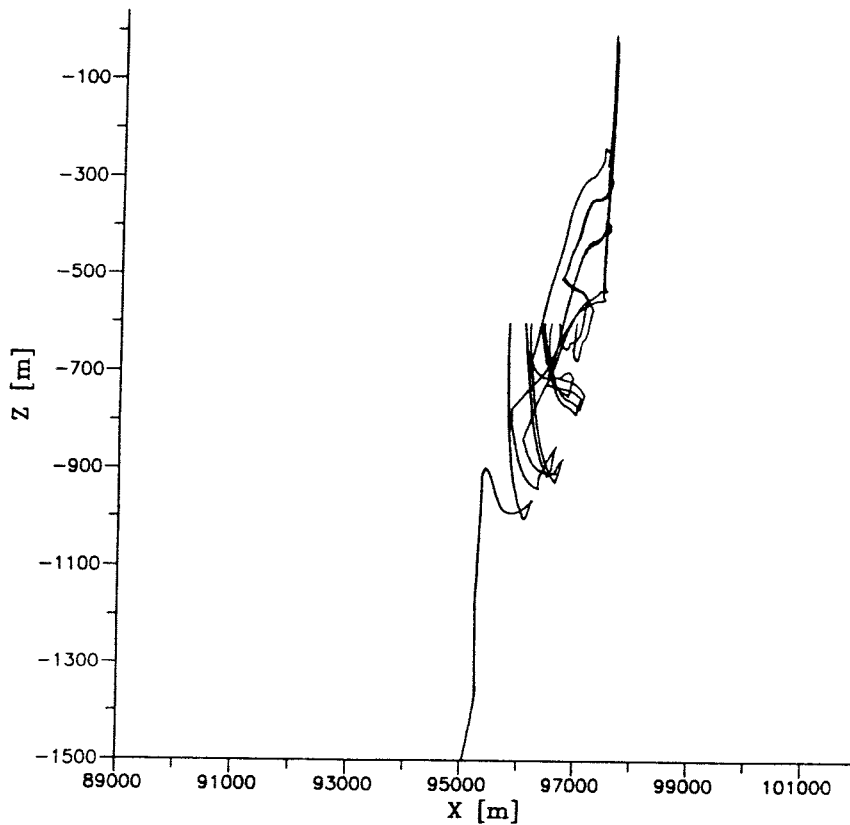
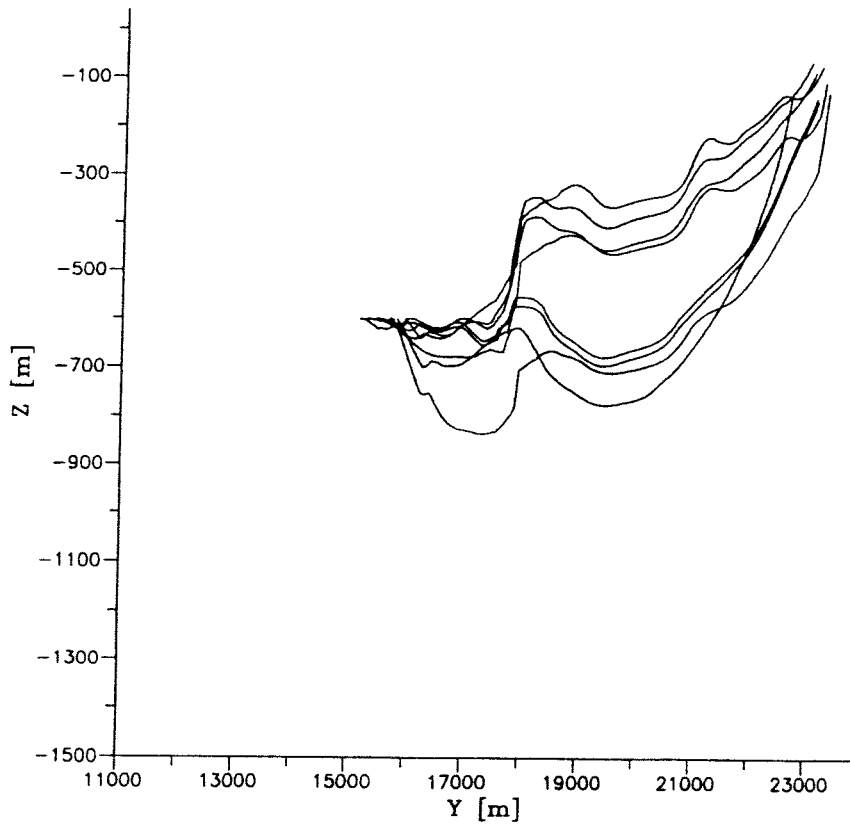**Figure B8**   *Vertical projection (xz-plane) of pathlines for Case X36GRV2.*

Figure B9   *Vertical projection (yz-plane) of pathlines for Case X36GRV2.*
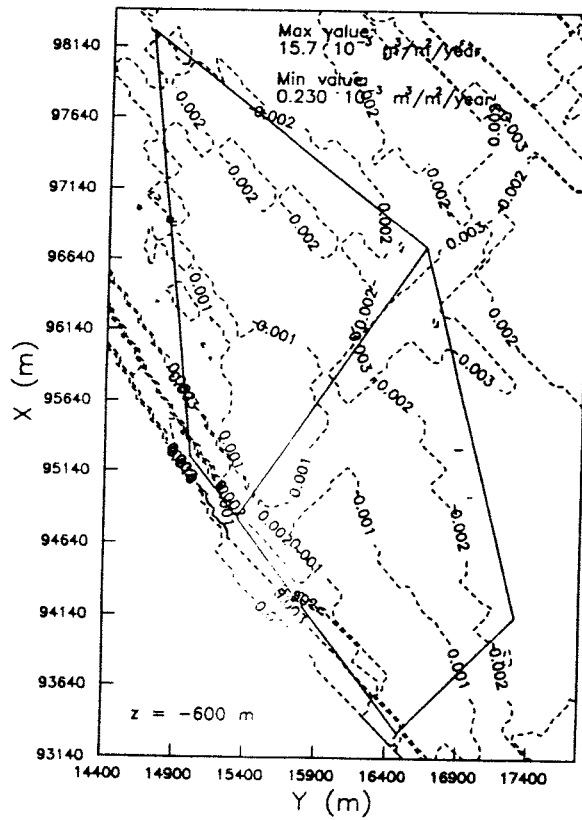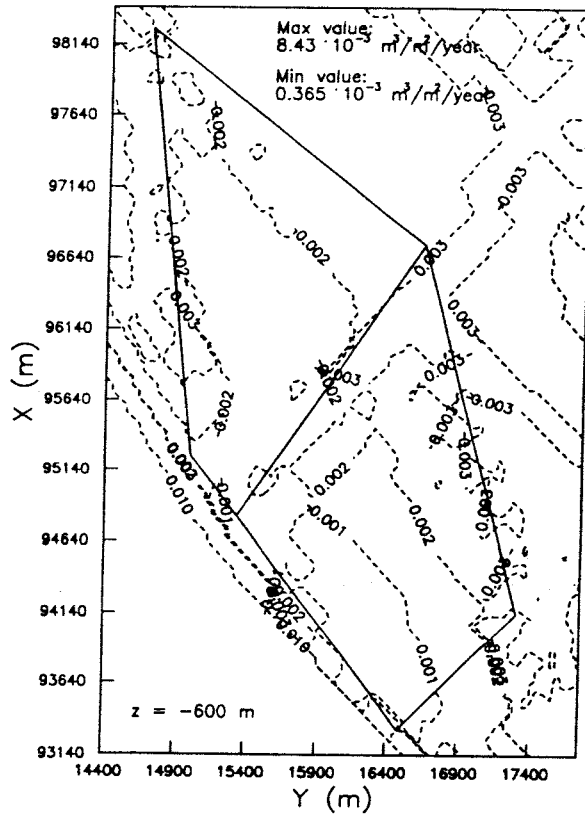

Figure B10   *Contoured flux distribution (m³/m²/year) for Case X36GRV2.*
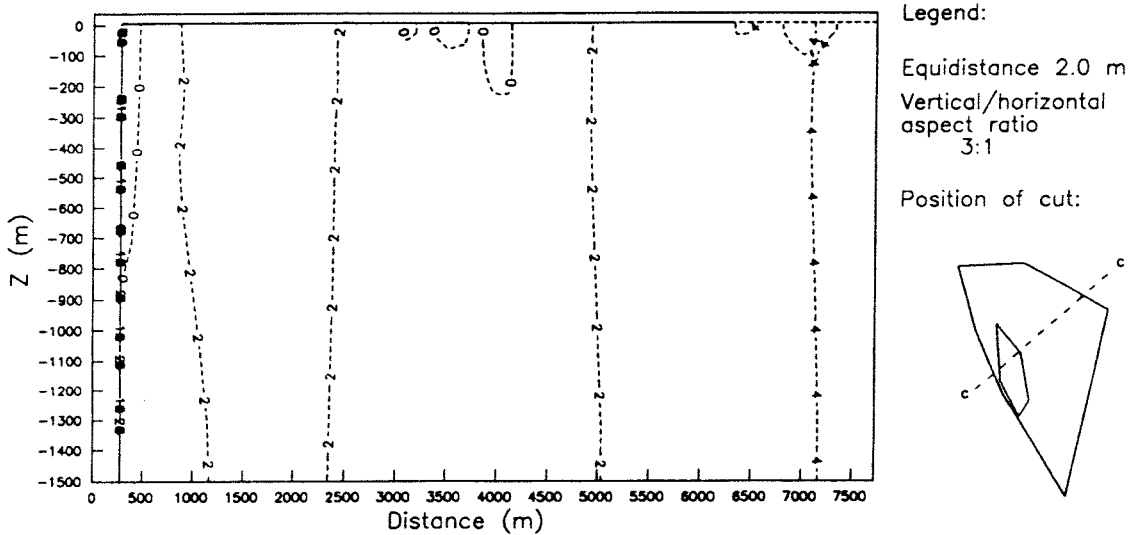
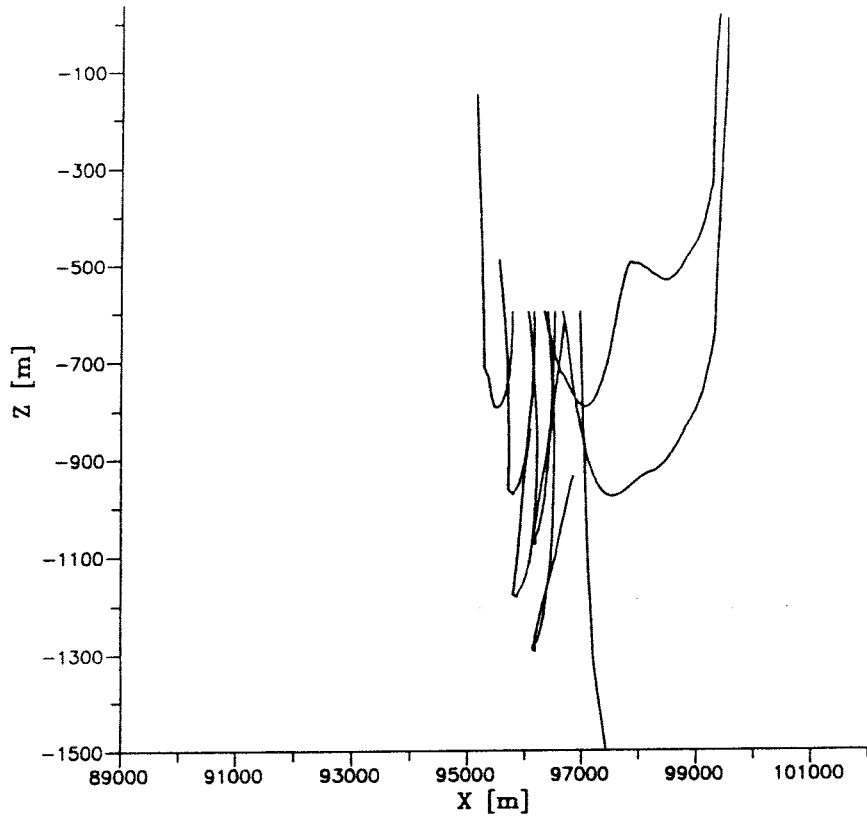*Figure B11   Distribution of hydraulic head in a vertical cross-section for Case X36GRV3.*
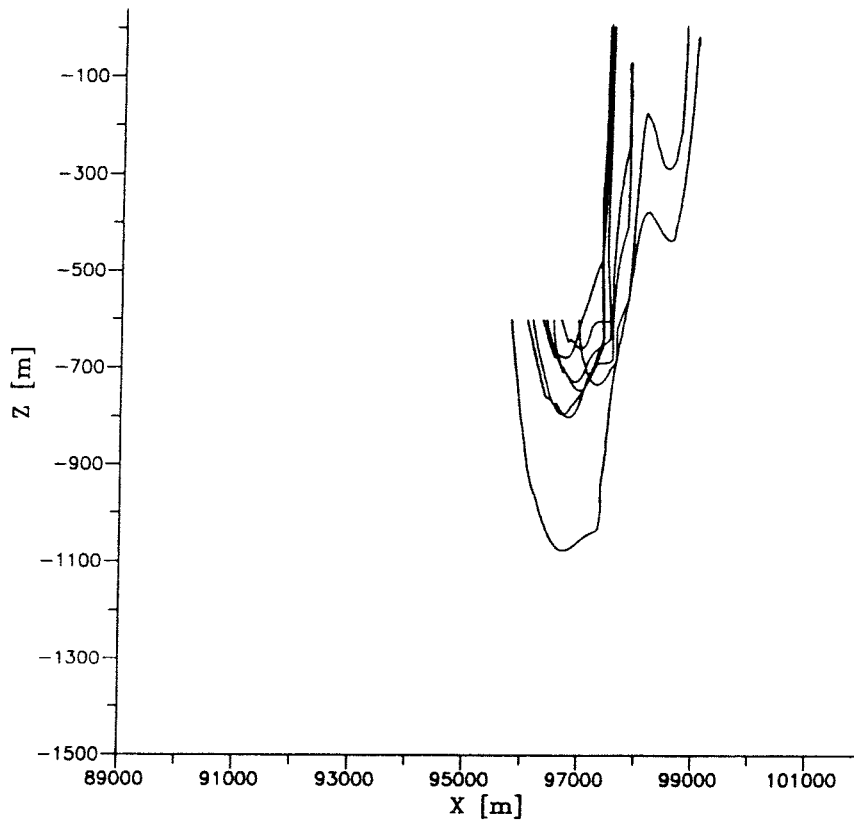
Figure B12   Vertical projection (xz-plane) of pathlines for Case X36GRV3.

Figure B13   *Vertical projection (yz-plane) of pathlines for Case X36GRV3.*
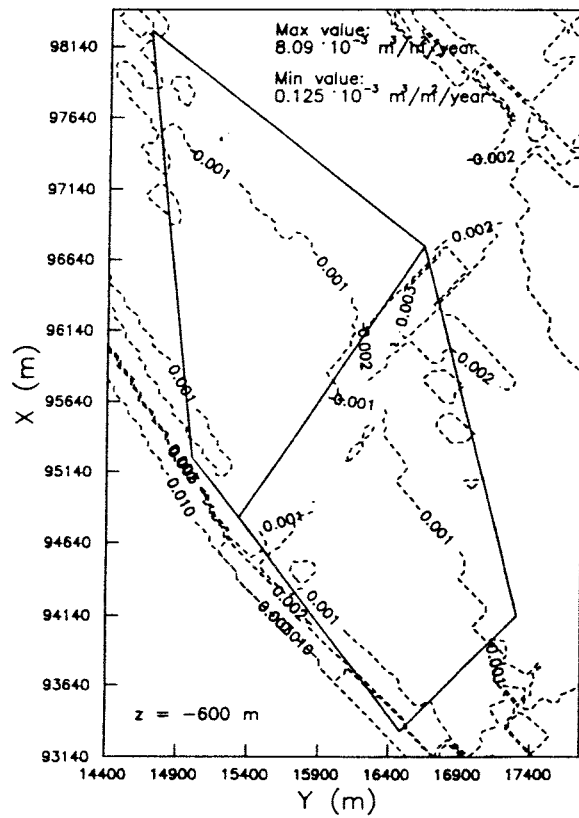
Figure B14   *Contoured flux distribution (m³/m²/year) for Case X36GRV3.*
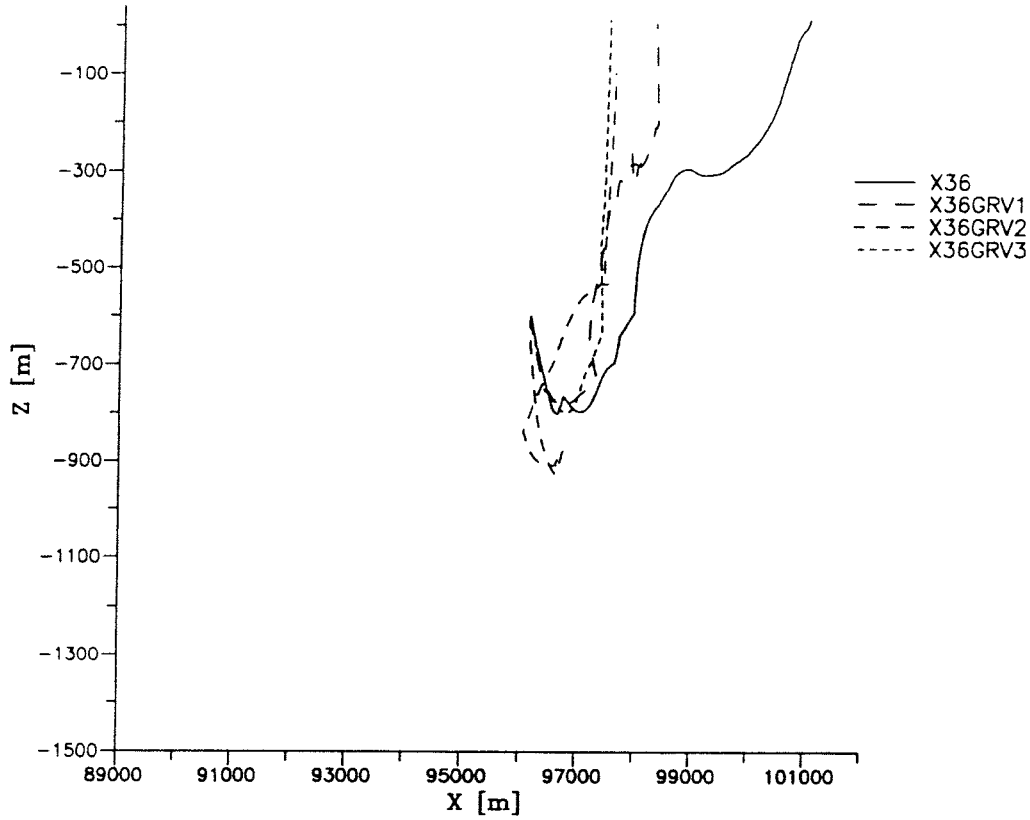
Figure B15   Vertical projection (xz-plane) of particle 7 for the Cases X36GRV1, X36GRV2 and X36GRV3.

Figure B16   Distribution of hydraulic head in a vertical cross-section for Case X36GRV4.

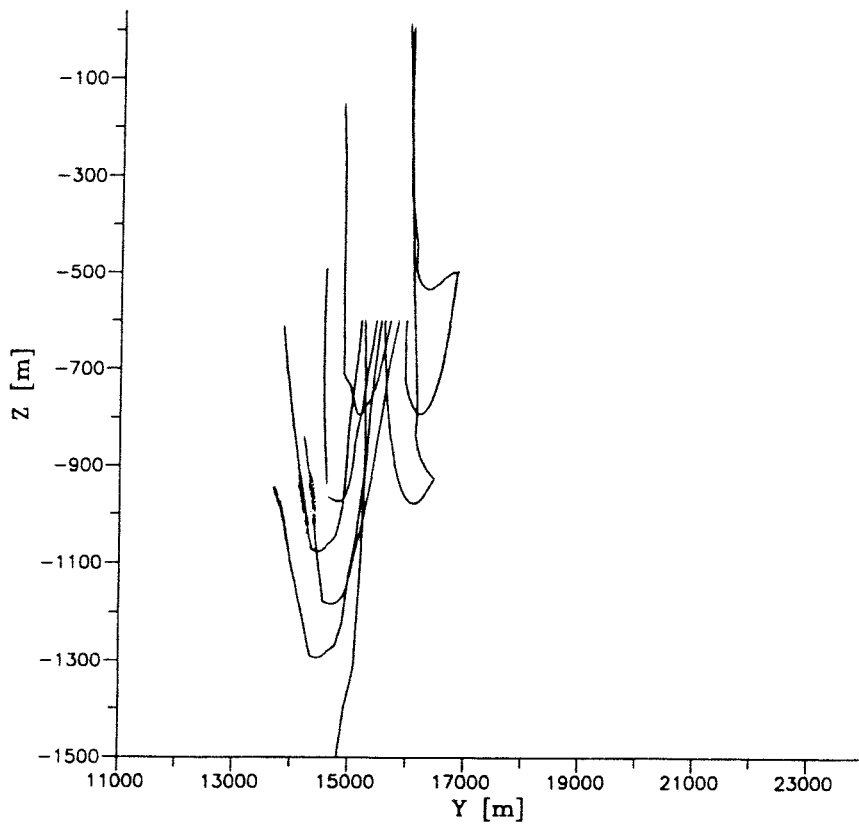*Figure B17*   *Vertical projection (xz-plane) of pathlines for Case X36GRV4.*

Figure B18   *Vertical projection (yz-plane) of pathlines for Case X36GRV4.*

Figure B19   *Contoured flux distribution (m³/m²/year) for Case X36GRV4.*

Figure B20   *Distribution of hydraulic head in a vertical cross-section for Case X36GRV5.*

Figure B21   *Vertical projection (xz-plane) of pathlines for Case X36GRV5.*

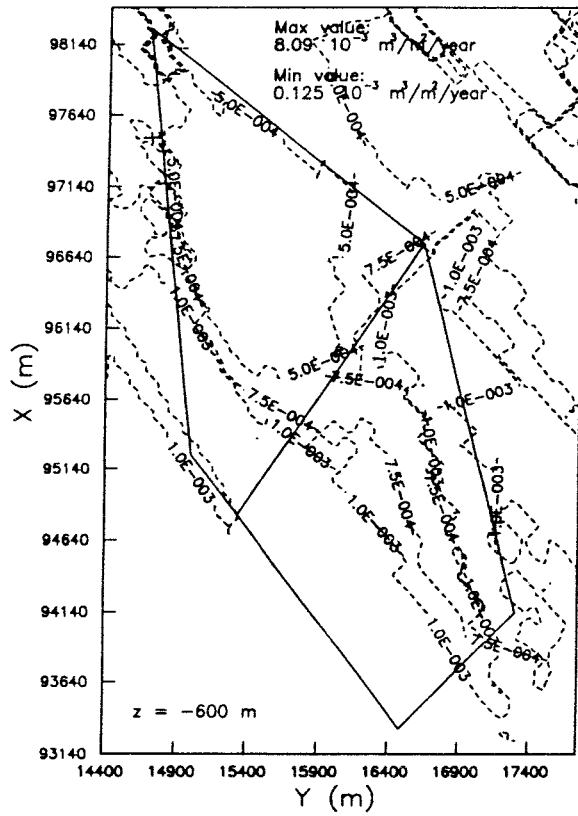*Figure B22*   *Vertical projection (yz-plane) of pathlines for Case X36GRV5.*

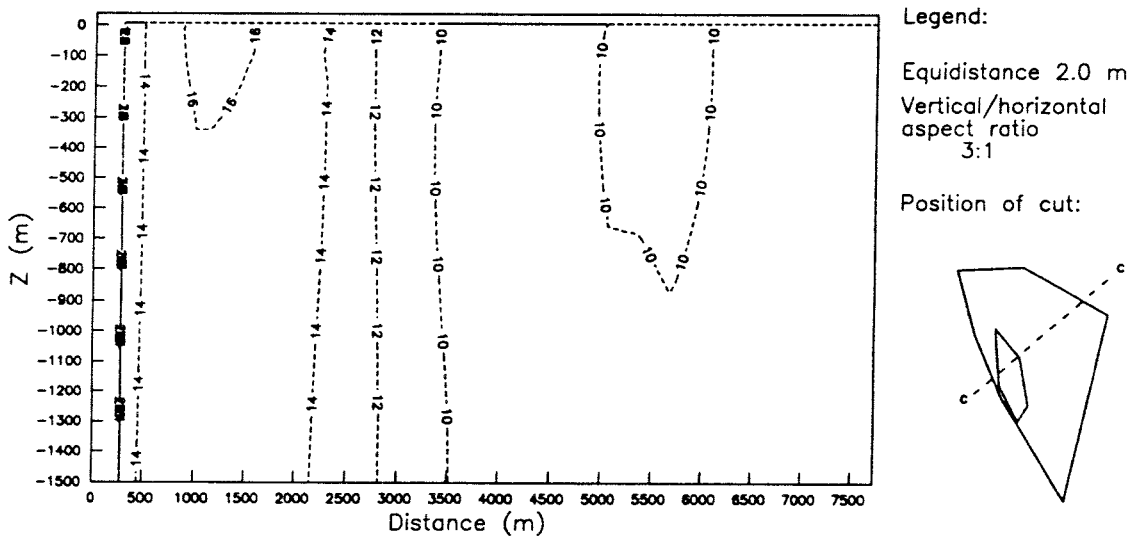*Figure B23   Contoured flux distribution (m³/m²/year) for Case X36GRV5.*

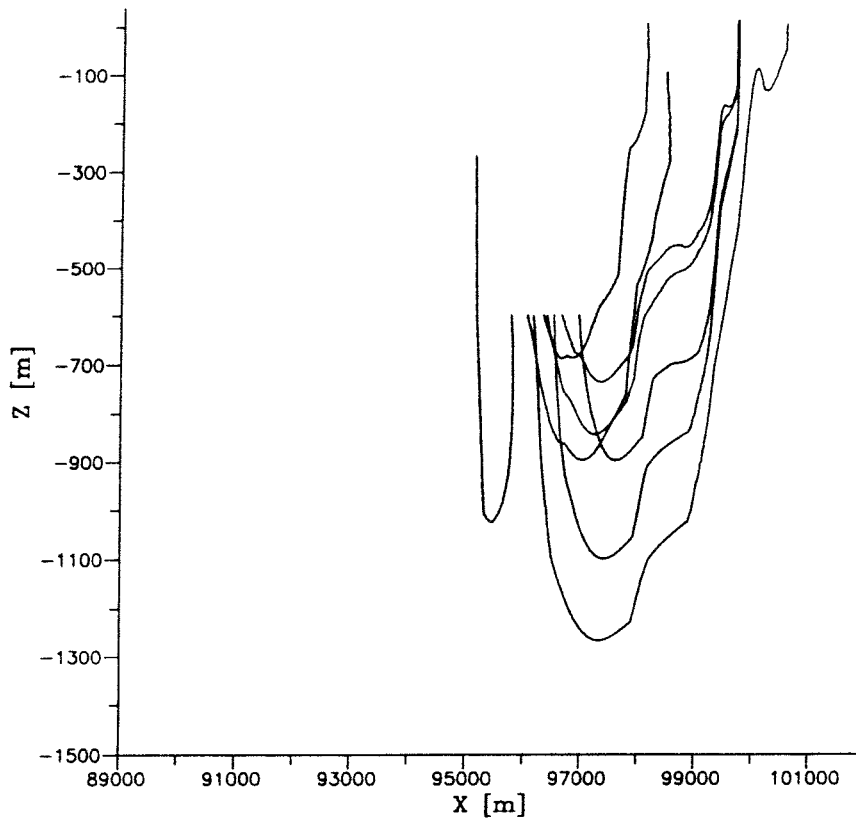*Figure B24   Distribution of hydraulic head in a vertical cross-section for Case X36GRV6.*

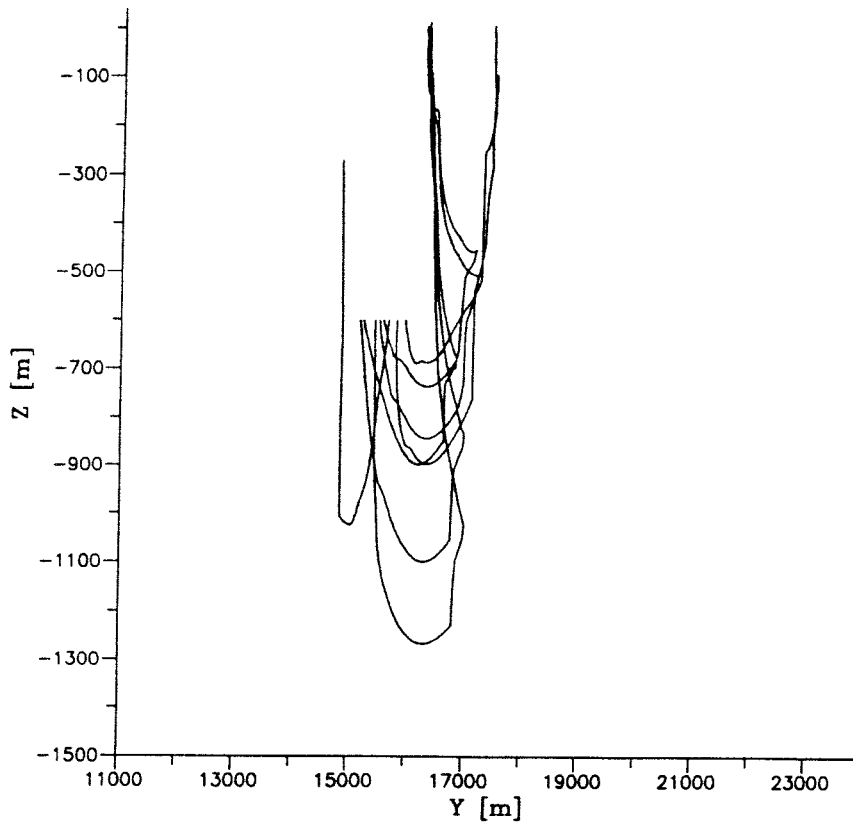*Figure B25*   *Vertical projection (xz-plane) of pathlines for Case X36GRV6.*

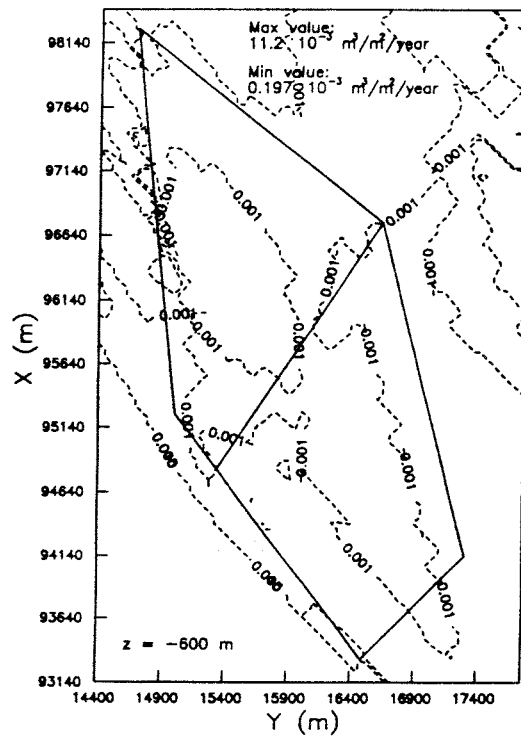*Figure B26*   *Vertical projection (yz-plane) of pathlines for Case X36GRV6.*

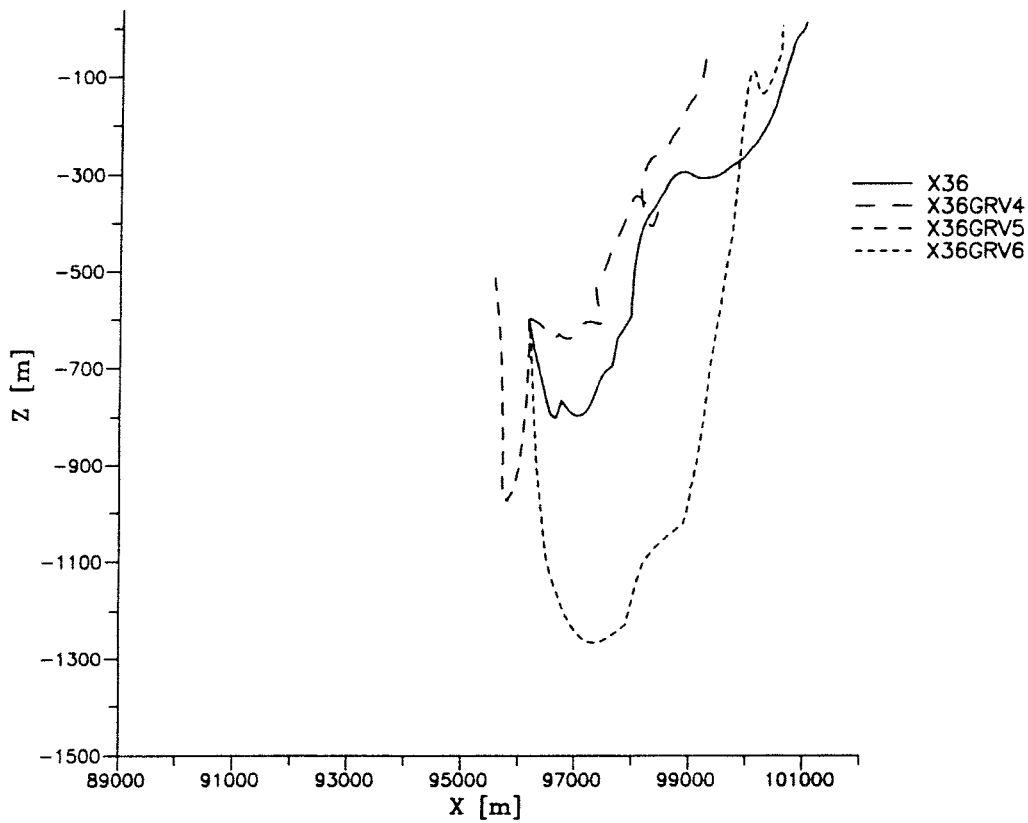*Figure B27*   *Contoured flux distribution ($m^3/m^2/year$) for Case X36GRV6.*

Figure B28   *Vertical projection (xz-plane) of particle 7 for the Cases X36GRV4, X36GRV5 and X36GRV6.*

List of SKB reports

Annual Reports

1977-78
TR 121
KBS Technical Reports 1 – 120
Summaries
Stockholm, May 1979

1979
TR 79-28
The KBS Annual Report 1979
KBS Technical Reports 79-01 – 79-27
Summaries
Stockholm, March 1980

1980
TR 80-26
The KBS Annual Report 1980
KBS Technical Reports 80-01 – 80-25
Summaries
Stockholm, March 1981

1981
TR 81-17
The KBS Annual Report 1981
KBS Technical Reports 81-01 – 81-16
Summaries
Stockholm, April 1982

1982
TR 82-28
The KBS Annual Report 1982
KBS Technical Reports 82-01 – 82-27
Summaries
Stockholm, July 1983

1983
TR 83-77
The KBS Annual Report 1983
KBS Technical Reports 83-01 – 83-76
Summaries
Stockholm, June 1984

1984
TR 85-01
Annual Research and Development Report 1984
Including Summaries of Technical Reports Issued
during 1984. (Technical Reports 84-01 – 84-19)
Stockholm, June 1985

1985
TR 85-20
Annual Research and Development Report 1985
Including Summaries of Technical Reports Issued
during 1985. (Technical Reports 85-01 – 85-19)
Stockholm, May 1986

1986
TR 86-31
SKB Annual Report 1986
Including Summaries of Technical Reports Issued
during 1986
Stockholm, May 1987

1987
TR 87-33
SKB Annual Report 1987
Including Summaries of Technical Reports Issued
during 1987
Stockholm, May 1988

1988
TR 88-32
SKB Annual Report 1988
Including Summaries of Technical Reports Issued
during 1988
Stockholm, May 1989

1989
TR 89-40
SKB Annual Report 1989
Including Summaries of Technical Reports Issued
during 1989
Stockholm, May 1990

1990
TR 90-46
SKB Annual Report 1990
Including Summaries of Technical Reports Issued
during 1990
Stockholm, May 1991

1991
TR 91-64
SKB Annual Report 1991
Including Summaries of Technical Reports Issued
during 1991
Stockholm, April 1992

Technical Reports
List of SKB Technical Reports 1992

TR 92-01
GEOTAB. Overview
Ebbe Eriksson[1], Bertil Johansson[2], Margareta
Gerlach[3], Stefan Magnusson[2], Ann-Chatrin Nils-
son[4], Stefan Sehlstedt[3], Tomas Stark[1]
[1]SGAB, [2]ERGODATA AB, [3]MRM Konsult AB
[4]KTH
January 1992

TR 92-02
Sternö study site. Scope of activities and main results
Kaj Ahlbom[1], Jan-Erik Andersson[2], Rune Nordqvist[2], Christer Ljunggren[3], Sven Tirén[2], Clifford Voss[4]
[1]Conterra AB, [2]Geosigma AB, [3]Renco AB,
[4]U.S. Geological Survey
January 1992

TR 92-03
Numerical groundwater flow calculations at the Finnsjön study site – extended regional area
Björn Lindbom, Anders Boghammar
Kemakta Consultants Co, Stockholm
March 1992

TR 92-04
Low temperature creep of copper intended for nuclear waste containers
P J Henderson, J-O Österberg, B Ivarsson
Swedish Institute for Metals Research, Stockholm
March 1992

TR 92-05
Boyancy flow in fractured rock with a salt gradient in the groundwater – An initital study
Johan Claesson
Department of Building Physics, Lund University, Sweden
February 1992

TR 92-06
Characterization of nearfield rock – A basis for comparison of repository concepts
Roland Pusch, Harald Hökmark
Clay Technology AB and Lund University of Technology
December 1991

TR 92-07
Discrete fracture modelling of the Finnsjön rock mass: Phase 2
J E Geier, C-L Axelsson, L Hässler, A Benabderrahmane
Golden Geosystem AB, Uppsala, Sweden
April 1992

TR 92-08
Statistical inference and comparison of stochastic models for the hydraulic conductivity at the Finnsjön site
Sven Norman
Starprog AB
April 1992

TR 92-09
Description of the transport mechanisms and pathways in the far field of a KBS-3 type repository
Mark Elert[1], Ivars Neretnieks[2], Nils Kjellbert[3], Anders Ström[3]
[1]Kemakta Konsult AB
[2]Royal Institute of Technology
[3]Swedish Nuclear Fuel and Waste Management Co
April 1992

TR 92-10
Description of groundwater chemical data in the SKB database GEOTAB prior to 1990
'Sif Laurent[1], Stefan Magnusson[2], Ann-Chatrin Nilsson[3]
[1]IVL, Stockholm
[2]Ergodata AB, Göteborg
[3]Dept. of Inorg. Chemistry, KTH, Stockholm
April 1992